

EVM Mitigation with PAPR and ACLR Constraints in Large-Scale MIMO-OFDM Using TOP-ADMM

Shashi Kant, *Graduate Student Member, IEEE*, Mats Bengtsson, *Senior Member, IEEE*, Gabor Fodor, *Senior Member, IEEE*, Bo Göransson, *Member, IEEE*, and Carlo Fischione, *Senior Member, IEEE*

Abstract—Although signal distortion-based peak-to-average power ratio (PAPR) reduction is a feasible candidate for orthogonal frequency division multiplexing (OFDM) to meet standard/regulatory requirements, the error vector magnitude (EVM) stemming from the PAPR reduction has a deleterious impact on the performance of high data-rate achieving multiple-input multiple-output (MIMO) systems. Moreover, these systems must constrain the adjacent channel leakage ratio (ACLR) to comply with regulatory requirements. Several recent works have investigated the mitigation of the EVM seen at the receivers by capitalizing on the excess spatial dimensions inherent in the large-scale MIMO that assume the availability of perfect channel state information (CSI) with spatially uncorrelated wireless channels. Unfortunately, practical systems operate with erroneous CSI and spatially correlated channels. Additionally, most standards support user-specific/CSI-aware beamformed and cell-specific/non-CSI-aware broadcasting channels. Hence, we formulate a robust EVM mitigation problem under channel uncertainty with nonconvex PAPR and ACLR constraints catering to beamforming/broadcasting. To solve this formidable problem, we develop an efficient scheme using our recently proposed three-operator alternating direction method of multipliers (TOP-ADMM) algorithm and benchmark it against two three-operator algorithms previously presented for machine learning purposes. Numerical results show the efficacy of the proposed algorithm under imperfect CSI and spatially correlated channels.

Index Terms—nonconvex PAPR reduction, Three-operator ADMM (TOP-ADMM), EVM, ACLR, MIMO-OFDM

I. INTRODUCTION

Modern mobile and wireless communication systems, such as 5G new radio (NR) and beyond, adopt orthogonal frequency division multiplexing (OFDM) with a cyclic prefix [2]. This is because of both its backward compatibility with 4G long-term evolution (LTE) as well as the fact that OFDM has several appealing attributes, such as robustness against the adverse effects of time and/or frequency selective channels, simplicity in terms of single-tap (frequency-domain) equalization, and resilience in terms of supporting both low and high symbol rates—thereby supporting various quality of service requirements.

It is well-known that OFDM suffers from high peak-to-average power ratio (PAPR) because of the linear combination of the subcarriers carrying (pseudo-random) M -ary quadrature

amplitude modulation symbols in the inverse discrete Fourier transform (IDFT) operation [3]. With the trend of an increasing number of transmit antennas and support of wider carrier bandwidths with the higher spectrum and spectral efficiencies, including support of higher frequency bands, the implementation of radio base station faces many challenges, notably in terms of power consumption and size—primarily dominated by power amplifiers (PAs). Thus, to reduce the power consumption of radio base stations or PAs, one must reduce the PAPR of the transmit signals for each transmit antenna. Additionally, the challenges are to support multiple radio access technologies, *e.g.*, 5G NR, 4G LTE, and narrowband internet of things (NB-IoT), by the same radio base station—where NB-IoT carriers can be placed in the guard bands of NR/LTE. For some classes of base stations, high average transmit output power of the signals is required for better cell coverage. Therefore, if PAPR is high and the required average transmit signal power is high, smaller size and efficient PA can cause non-linear distortions rendering both inband and out-of-band emissions (OOBE)—which may fail the base station to comply with 3rd Generation Partnership Project (3GPP) standard and regulatory requirements. Consequently, if PAPR is kept high, an inefficient and bigger size PA will be employed such that the signals can operate in a linear region to avoid non-linear distortions. Hence, it is paramount to minimize the PAPR of OFDM waveform in large-scale multiple-input multiple-output (MIMO) systems. Furthermore, low PAPR of the signals with a digital predistorter or a PA linearizer can improve the PA efficiency by letting PA operate close to its bias point.

Numerous techniques to reduce PAPR, also referred to as crest factor reduction, have been proposed in the literature over the past decades. These can be grouped as 1) distortion-based approaches, such as iterative clipping and filtering [4], [5], peak cancellation [6], [7], and non-linear companding [8]; 2) coding-based methods [9]; and 3) multiple signaling-based approaches, such as selected mapping, partial transmit sequences [10], and tone reservation [11] (see also review papers [12]–[14]). Distortion-based techniques, particularly clipping and filtering, are the most popular methods in practice as they are transparent to the standards and to the receiver, see [13]. However, they cause significant in-band distortion—quantified in terms of error vector magnitude (EVM)—and may increase OOBE. Basically, these distortion-based techniques manage the inherent trade-off between EVM and achievable PAPR. More precisely, if the desired PAPR threshold is low, then the inband transmit EVM is high, which consequently penalizes the throughput performance at the receiver.

S. Kant, B. Göransson, and G. Fodor are with Ericsson AB and KTH Royal Institute of Technology, Stockholm, Sweden (e-mail: {shashi.v.kant, bo.goransson, gabor.fodor}@ericsson.com)

M. Bengtsson and C. Fischione are with KTH Royal Institute of Technology, Stockholm, Sweden (e-mail: {matben, carlofi}@kth.se)

The work of S. Kant was supported in part by the Swedish Foundation for Strategic Research under grant ID17-0114.

Parts of this work is presented at IEEE Asilomar 2021 [1].

II. RELATED WORKS AND CONTRIBUTIONS

In this section, we first give an overview of some prior works on PAPR reduction methods with some practical challenges for 5G NR and beyond to motivate distortion-based PAPR techniques. Most of the principled approaches for distortion-based PAPR reductions are posed as optimization problems, whose (near-)optimal solutions cannot be obtained in closed-form and require efficient iterative optimization techniques to tackle the problem. Thus, we briefly describe some powerful and efficient first-order optimization techniques to tackle the PAPR reduction problems for large-scale MIMO-OFDM-based systems. Finally, we highlight our original contribution with mathematical notations and paper organization.

A. Practical Research Challenges for PAPR Reduction Techniques in 5G NR and Beyond

As mentioned above, the base station supports multiple standards from 4G LTE to current 5G NR releases, including cellular internet of things (IoT), possibly in the guard bands of LTE/NR. It supports wide bandwidths and multiple bands with growing demand for energy-efficient and lightweight radio heads of the base stations equipped with many transmit antennas. Clearly, PAPR of the multiple carriers of the signals must be reduced, which complements PA linearization such as digital predistortion to improve PA efficiency—targeting energy-efficient and lightweight base stations. The challenges for the PAPR reduction techniques are that 1) one cannot exploit guard bands to deploy many non-useful subcarriers for PAPR reduction such as in tone reservation [11], and 2) one cannot send extra non-standard side information to the receiver(s) because of compliance with the stringent 3GPP standard and regulatory requirements.

B. Related Works for PAPR Reduction Techniques

We briefly summarize some of the related works for PAPR reduction in OFDM-based systems, including MIMO, wherever applicable. Moreover, we refer interested readers to overview papers [12]–[14].

1) Multiple Signaling and Probabilistic Methods: These techniques reduce PAPR by either generating multiple permutations, introducing phase shifts or adding peak reducing subcarriers of OFDM signal.

Selective mapping [12]–[15] generates multiple statistically independent input data sequences representing the same useful information, where the generated signal with the lowest PAPR is selected for the transmission. However, the receiver must know the chosen mapping at the transmitter for successful demodulation of the signal via side information. Hence, unfortunately, selective mapping cannot be employed in 3GPP-compliant cellular base stations. There are some related methods to selective mapping, called partial transmit sequences—see [12]–[14] and references therein.

Tone reservation [11]–[14], [16] is one of the signal distortion-less techniques for PAPR reduction, which utilizes unused/inactive subcarriers—that is, adds peak reducing

subcarriers—typically in the vicinity of used/active subcarriers carrying useful information. On the one hand, one of the strengths of tone reservation is that it does not induce any signal distortions on the useful data-carrying subcarriers. On the other hand, although tone reservation offers low complexity, as discussed above, unfortunately, the limited number of unused/inactive subcarriers can be exploited because of relatively high spectrum efficiency of 5G NR compared to LTE and nearly no effective guard bands are available in 5G NR (or even LTE) as NB-IoT carriers can also be deployed in the guard bands of NR/LTE. Nevertheless, ignoring the guard band usage restrictions of NR/LTE, in Section V-B, we have evaluated and compared the performance of two variants of tone reservation schemes against our proposed method—see particularly Fig. 4.

2) Coding-based PAPR Reduction: These coding-based techniques, *e.g.*, linear block codes, Golay complementary sequences, and turbo coding—see [12]–[14] and references therein—reduce the PAPR by generating encoded data inputs that produce an OFDM symbol with desired PAPR. However, these techniques typically require an exhaustive search for a good code, which becomes intractable for an OFDM-based system with more than a dozen subcarriers. Unfortunately, such techniques are practically impossible with a 5G NR-like system.

3) Distortion-based PAPR Reduction: These distortion-based methods essentially reduce the PAPR by (non-linear) distortion of the useful transmit signal, where the signal quality degradation is measured in terms of EVM. Moreover, these distortion-based methods render OOB, which must be handled via appropriate filtering in either time or frequency domain.

Active constellation or active set extension [17] reduces PAPR by modifying or (pre)distorting the modulation constellation carried on the useful/active subcarriers with a minimal penalty in terms of EVM. Although no side information needs to be sent to the receiver, this method has, unfortunately, limited application to large modulation alphabet, *e.g.*, alphabet size more than 64QAM [12], [13]. Hence, active constellation extension is not feasible for a 5G NR-like system where more than 64QAM, *e.g.*, 256/1024QAM, modulation alphabet can be supported.

Iterative clipping and filtering [4], [5] is one of the simplest approaches, which clips the high amplitudes of the signal if above a given peak threshold while retaining the phase of the signals. This peak clipping causes unwanted distortions inband and out-of-band—*i.e.*, EVM and OOB. This induced OOB needs to be filtered out either in frequency or time domain to maintain desired 3GPP adjacent channel leakage ratio (ACLR) requirements. Consequently, filtering of unwanted distortions causes regrowth of the signal peaks. However, after a few repetitions/iterations of clipping and filtering reduces PAPR but at the cost of increased signal distortion (EVM) depending on the chosen peak threshold. If the signal peaks are clipped at a lower threshold, signal distortion—EVM—increases significantly, penalizing the throughput [18].

Recently, for reciprocity-based or channel state information (CSI)-aware massive/large-scale MIMO, distortion-based PAPR reduction techniques, see, e.g., [18]–[22], are proposed, which not only reduce the PAPR at the transmitter but also mitigate the incurred signal distortion (EVM) seen at the receiver by exploiting downlink channel knowledge available at the base station. Most of these distortion-based techniques relax the nonconvex PAPR problem by employing either minimization of peaks, see, e.g., [18], which renders a suboptimal solution, or semidefinite relaxation, see, e.g., [20], which can enable a near-optimal solution at the expense of prohibitive computational complexity. Another drawback is that many of these methods are not robust when the downlink channel knowledge acquired at the transmitter is either imperfect or incomplete e.g., [19], [21], [22]. Several of these previously proposed methods lack the flexibility to adapt the desired PAPR target and OOB—typically quantified in terms of ACLR—according to the regulatory requirements. Furthermore, in realistic systems, the channel estimates at the transmitter and receiver are imperfect and/or incomplete. Consequently, under imperfect and/or incomplete channel estimates, these previously proposed non-robust schemes cannot achieve (near) zero EVM at the receiver (as shown in Section V). Additionally, these non-robust prior arts do not support the incomplete channel knowledge case, that is, OFDM symbols carrying broadcast channels (such as cell-specific control channels), since there is no downlink channel knowledge as these common channels naturally do not target a specific subset of the served users. Although [20] offers various robust methods for reciprocity-based PAPR reduction techniques, in these schemes there is no constraint on OOB or ACLR, which are important for PAPR reduction schemes. Additionally and regrettably, semidefinite programming-based algorithms are typically solved by interior-point-based methods [23], which have prohibitive complexity for state-of-the-art base station radio hardware systems.

C. Motivation for Distortion and Optimization Based PAPR Reduction

Considering practical constraints/restrictions in 5G NR and beyond, an interesting candidate is a distortion-based PAPR reduction scheme, which utilizes mainly useful/active subcarriers to reduce the PAPR of the OFDM signal. Concretely, we seek a one-size-fits-all PAPR reduction scheme that can naturally work for base stations equipped with single or multiple transmit antennas and adaptively caters to non-CSI-aware, e.g., broadcast channels, and CSI-aware if possible. In large-scale MIMO, the base station has a large number of antennas compared to the total number of served/scheduled spatial layers for the transmission—applicable to both single-user MIMO (SU-MIMO) or multi-user MIMO (MU-MIMO)—and additionally has some good enough quality of downlink channel estimates of all the served users. Consequently, one could potentially relax the EVM requirements at the transmitter stipulated by the standards, such as 3GPP NR [24], by mitigating/reducing the EVM seen at the receivers of the users accordingly while meeting the desired PAPR and ACLR requirements

at the transmitter of a base station. Moreover, if the base station has no downlink channel knowledge of the users for instance supporting broadcast or control channels in some OFDM symbols over all the active subcarriers within a bandwidth, we propose minimizing the signal distortion energy subject to the desired PAPR and ACLR constraints. Additionally, we seek a principled approach to describe the distortion-based PAPR reduction scheme using an optimization formulation and subsequently develop a (near-)optimal and computationally-efficient solution. In practice, we do not require highly accurate solution, especially for the problems of interest in this work. Therefore, the subsequent section introduces first-order optimization schemes, which offer a good trade-off between computational complexity and accuracy. Hence, these first-order methods can tackle complicated composite problems and yield implementation-friendly algorithms suitable for large-scale MIMO-OFDM systems.

D. Related Works on Operator/Proximal Splitting for Signal Processing in Communications

In the optimization problems mentioned above, proximal/operator splitting techniques—typically first-order optimization algorithms—have become popular thanks to their low computational complexity. This can be seen not only in wireless communications but also in machine learning applications. Operator splitting methods employ a divide-and-conquer approach, which essentially breaks the large problem into smaller, easy-to-solve subproblems. However, first-order methods can be very slow to converge to solutions having high accuracy. Nonetheless, modest accuracy can be sufficient for many practical applications, such as in this work. There is a plethora of proximal/operator splitting methods [25]–[34] to tackle the generic composite problems. The operator splitting algorithms can be roughly grouped into two classes of algorithms [33], namely primal-dual-type—e.g., Chambolle-Pock-type [29]—and primal/dual-type—e.g., alternating direction method of multipliers (ADMM)-type [34] algorithms.

Operator splitting for two operators (or, loosely speaking, optimization problems in which the objective function is given by the sum of two functions) has been widely studied [25]–[27], [29]–[31], [34]. Operator splitting with more than two composite terms in the objective has been an active research problem without resorting to problem or product space reformulations [32] because these techniques are either not straightforward or converge slowly [32], [33]. In other words, if the optimization problem comprises more than two functions, then under certain separability and smoothness assumptions, a typical approach is to reformulate the problem by modeling it as a block-wise two-operator problem such that one can exploit the separability of grouped functions within each block. However, as shown in [32], [33], [35], this can lead to slow convergence or/and exhibit memory inefficiency. Therefore, novel algorithms are researched and developed to solve composite problems comprising more than two operators.

Related Works on Three-Operator Splitting: Recently, some authors have extended both primal/dual-type (including ADMM-type) algorithms and primal-dual classes of splitting

algorithms from two operators to three operators [28], [32]–[37]. ADMM (primal-/dual-type splitting) algorithms for three operators have gained interest in the literature. There are many varieties of ADMM in the literature, see, *e.g.*, [30]. One of the popular variants is the so-called proximal ADMM, which essentially regularizes each subproblem with a quadratic proximal regularization (or weighted norm). A special case of proximal ADMM is linearized proximal ADMM, which basically cancels out the inconvenient quadratic terms in the subproblem. However, “linearization” in the ADMM-type literature can be ambiguous [34]. Besides the aforementioned linearization of the subproblem, there are also techniques that linearize the L -smooth¹ objective function within the ADMM-type class of algorithms designed to solve the three-operator problem [28], [32], [35], [36], which we collectively refer to as three-operator ADMM (TOP-ADMM)-type algorithms in this work.

E. Contribution

In this paper, we develop scalable, flexible, and computationally efficient optimization methods to tackle a robust and nonconvex PAPR reduction problem while catering to both beamforming and broadcasting in standard-compliant wireless communication systems such as 5G NR. Our contributions are as follows:

- We formulate a PAPR reduction optimization problem amenable to large-scale MIMO-OFDM, where the transmit distortion (or EVM) stemming from the PAPR reduction subproblem is mitigated at the receiver without imposing any additional signal processing requirement at the receiver.
- Additionally, the proposed problem formulation offers flexibility to adapt the desired PAPR and ACLR targets, and can seamlessly support both beamforming and broadcasting carrying resources. Note that user-specific and common resources may exist in the same OFDM symbol. One could argue that it is not non-trivial to extend the previously proposed methods supporting both beamforming and broadcasting, particularly a special case of our proposed formulation.
- We introduce a powerful yet simple optimization solution algorithm based on our recently proposed TOP-ADMM method [35], which is intended for a class of three-operator proximal splitting schemes. To benchmark it against state-of-the-art algorithms, we also provide details on how to apply Bregman ADMM (BADMM) [1], [28] and Davis-Yin splitting (DYS) [32] to the problem at hand.
- We present simulation results for downlink 5G NR-like systems to substantiate the capability of the proposed TOP-ADMM-based algorithm. Additionally, we analyze the performance considering PAPR and EVM metrics under imperfect CSI available at the transmitter and considering spatially-correlated wireless channels.

¹See Definition 1 of L -smooth function.

F. Notation

Let the set of complex and real numbers be denoted by \mathbb{C} and \mathbb{R} , respectively. $\Re\{x\}$ denotes the real part of a complex number $x \in \mathbb{C}$. The i -th element of a vector $\mathbf{a} \in \mathbb{C}^{m \times 1}$ and j -th column vector of a matrix $\mathbf{A} \in \mathbb{C}^{m \times n}$ are denoted by $a[i] := (\mathbf{a})_i \in \mathbb{C}$ and $\mathbf{A}[:, j] \in \mathbb{C}^{m \times 1}$, respectively. An i -th element of three-order tensor is denoted in matrix form as $\mathbf{X}[i] \in \mathbb{C}^{m \times n}$. We form a matrix by stacking the set of higher order vectors $\{\mathbf{a}[n] \in \mathbb{C}^{M \times 1}\}_{n=1}^N$ and $\{\mathbf{b}[m] \in \mathbb{C}^{1 \times N}\}_{m=1}^M$ column-wise and row-wise as $\mathbf{A} = [\mathbf{a}[1], \dots, \mathbf{a}[N]] \in \mathbb{C}^{M \times N}$ and $\mathbf{B} = [\mathbf{b}[1]; \dots; \mathbf{b}[M]] \in \mathbb{C}^{M \times N}$, respectively. The transpose and conjugate transpose of a vector or matrix are denoted by $(\cdot)^T$ and $(\cdot)^H$, respectively. The complex conjugate is represented by $(\cdot)^*$. The $K \times K$ identity matrix is written as \mathbf{I}_K . The expectation operator is denoted by $\mathbb{E}\{\cdot\}$. An i -th iterative update is denoted by $(\cdot)^{(i)}$; $\mathbf{e}_k \in \mathbb{R}^{N \times 1}$ is a standard basis vector. \mathbf{F} refers to the discrete Fourier transform (DFT) matrix; $\mathbf{A}^{1/2}$ denotes the square root of \mathbf{A} .

G. Paper Organization:

The remainder of the paper is organized as follows. The next section briefly introduces the system and EVM model with useful performance and algorithm design metrics. Section IV formulates EVM mitigation with PAPR and ACLR constraints suitable for any practical 5G NR-like system, *i.e.*, supporting both user-specific and cell-specific signals. Moreover, in Section IV, we first introduce our novel TOP-ADMM algorithm as a generic splitting method and thereafter present an algorithm tackling the proposed large-scale problem using TOP-ADMM. Then, we also present the benchmark algorithms tackling the same proposed problem using BADMM [1], [28] and DYS [32]. Moreover, we characterize the computational complexities of these TOP-ADMM-type algorithms by solving the proposed problem and compare their complexities with two prior arts. Section V gives a rich set of numerical results, and Section VI concludes with a summary.

III. PRELIMINARIES

This section briefly introduces the downlink MIMO-OFDM system model followed by a short description of the performance metrics that are useful for designing distortion-based PAPR reduction algorithms.

A. System Model for Distortion-Based PAPR Reduction in Frequency-Domain

We consider an OFDM-based MIMO downlink—as depicted in Fig. 1—where the base station is equipped with N_T transmit (Tx) antennas, and the user equipment (UE) is equipped with N_R receive (Rx) antennas. Moreover, we assume a spatial multiplexing transmission scheme with $N_L \leq \min\{N_T, N_R\}$ spatial layers. For MU-MIMO, N_U represent total number of scheduled users sharing all the resources for the data transmission, where each μ -th user can have $N_{L_\mu} \leq N_L$ spatial layers such that $N_L = \sum_{\mu=1}^{N_U} N_{L_\mu}$.

A (generalized) spatially precoded (or beamformed) symbol matrix in frequency-domain input to an ℓ -times oversampled K -point IDFT matrix is denoted by $\mathbf{X} \in \mathbb{C}^{N_T \times \ell K}$ such that at

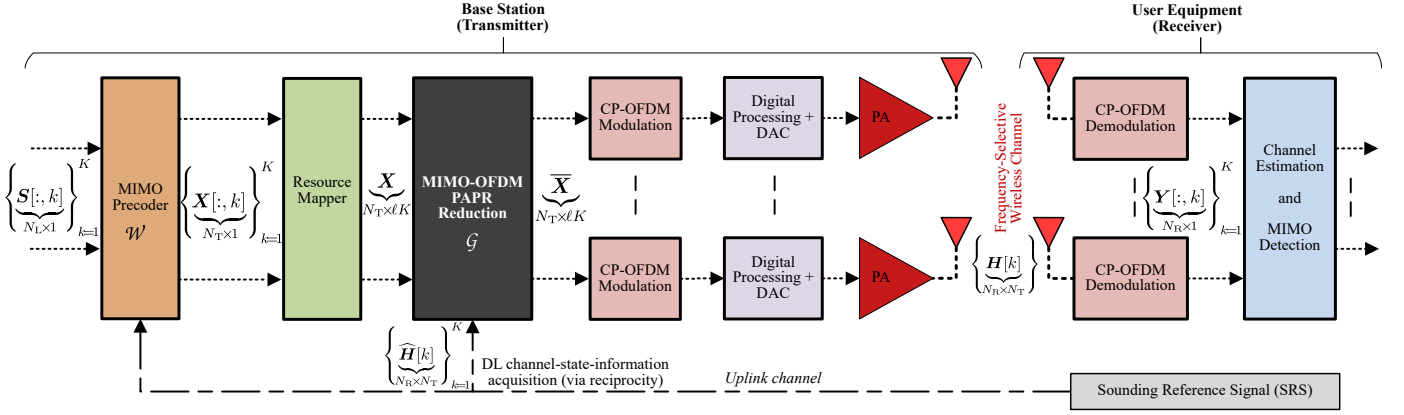


Fig. 1: Simplified block diagram of a single-user MIMO-OFDM transceiver with PAPR reduction scheme.

the k -th (useful) subcarrier, $\mathbb{C}^{N_T \times 1} \ni \mathbf{X}[:, k] = \mathcal{W}(\mathbf{S}[:, k])$, where non-precoded symbol vector, for all the spatial layers of SU-MIMO/MU-MIMO, $\mathbf{S}[:, k] \in \mathcal{S}^{N_L \times 1}$ belongs to a complex-valued finite-alphabet set \mathcal{S} , *e.g.*, corresponding to a 2^Q -quadrature amplitude modulation (QAM) constellation with $Q \in \{2, 4, 6, 8\}$. The spatial (possibly nonlinear) precoding $\mathcal{W} : \mathcal{S}^{N_L \times 1} \rightarrow \mathbb{C}^{N_T \times 1}$ maps the non-precoded symbol vector $\mathbf{S}[:, k] \in \mathcal{S}^{N_L \times 1}$ to spatially precoded symbol vector $\mathbf{X}[:, k] \in \mathbb{C}^{N_T \times 1}$ catering either SU-MIMO or MU-MIMO. For MU-MIMO, $\mathbf{S}[:, k] = [\mathbf{S}_1[:, k]; \dots; \mathbf{S}_{N_U}[:, k]]$, where $\mathbf{S}_\mu[:, k] \in \mathcal{S}^{N_{L_\mu} \times 1}$ represent μ -th user's data vector.

1) *Transmit SU/MU-MIMO Signal Model:* Inspired by, *e.g.*, [35], [38], we model a frequency-domain data matrix $\bar{\mathbf{X}}$ having reduced PAPR as $\mathbb{C}^{N_T \times LK} \ni \bar{\mathbf{X}} := \mathcal{G}(\mathbf{X})$, where a distortion-based PAPR reduction function $\mathcal{G} : \mathbf{X} \in \mathbb{C}^{N_T \times LK} \rightarrow \mathbb{C}^{N_T \times LK} \ni \bar{\mathbf{X}}$ manipulates the data symbol matrix \mathbf{X} . Consequently, this perturbation signal model capable of reducing PAPR at a given k -th subcarrier can be expressed as,

$$\bar{\mathbf{X}}[:, k] = \alpha[k] \mathbf{X}[:, k] + \underbrace{\boldsymbol{\epsilon}[k]}_{\text{Tx distortion}} \approx \mathbf{X}[:, k] + \boldsymbol{\epsilon}[k] \quad (1)$$

where $\alpha[k] \in \mathbb{C}$ is a deterministic scalar and $\boldsymbol{\epsilon}[k]$ is an instantaneous distortion that is uncorrelated with $\mathbf{X}[:, k]$ but statistically dependent. However, appealing to the works in [35], [39]–[42], $\boldsymbol{\epsilon}[k]$ stemming from any (possibly nonlinear) source, *e.g.*, clipping, spectral precoding, is correlated across antennas and consequently beamformed in the similar direction as the signal $\mathbf{X}[:, k]$, for instance, depending on the ratio of transmit spatial layers and the transmit antenna branches—*i.e.*, rank of the channel, frequency-granularity of the spatial precoding—*i.e.*, channel coherence bandwidth. Observe that although the scaling factor $\alpha[k]$ may vary across subcarriers, on average, the scaling is assumed to be real-valued and nearly unity—our extensive simulations in Section V show that the approximate additive EVM model (1) is accurate and ignoring $\alpha[k]$ has nearly negligible impact on the key performance metrics.

2) *Received SU/MU-MIMO Signal Model:* For MU-MIMO, let N_{R_μ} denote the number of receive antennas of user μ such that the total number of receive antennas for all the users is $N_R = \sum_{\mu=1}^{N_U} N_{R_\mu}$. Additionally, let $\mathbf{H}_\mu[k] \in \mathbb{C}^{N_{R_\mu} \times N_T}$ describe the channel matrix between user μ and base station such that the composite

channel matrix over all the receive antennas of users is $\mathbf{H}[k] = [\mathbf{H}_1[k]; \dots; \mathbf{H}_{N_U}[k]]$. Therefore, the received signal model of user μ can be expressed as

$$\mathbb{C}^{N_{R_\mu} \times 1} \ni \mathbf{Y}_\mu[:, k] = \mathbf{H}_\mu[k] \bar{\mathbf{X}}[:, k] + \mathbf{n}_\mu[k] \quad (2a)$$

$$\begin{aligned} &= \underbrace{\mathbf{S}_\mu[:, k]}_{\text{desired}} \\ &+ \underbrace{(\mathbf{H}_\mu[k] \bar{\mathbf{X}}[:, k] - \mathbf{S}_\mu[:, k])}_{\text{interuser interference and received Tx distortion}} \\ &+ \mathbf{n}_\mu[k], \end{aligned} \quad (2b)$$

$$\approx \mathbf{H}_\mu[k] \mathbf{X}[:, k] + \mathbf{H}_\mu[k] \boldsymbol{\epsilon}[k] + \mathbf{n}_\mu[k] \quad (3a)$$

$$\begin{aligned} &= \underbrace{\mathbf{S}_\mu[:, k]}_{\text{desired}} \\ &+ \underbrace{(\mathbf{H}_\mu[k] \mathbf{X}[:, k] - \mathbf{S}_\mu[:, k])}_{\text{interuser interference}} \\ &+ \underbrace{\mathbf{H}_\mu[k] \boldsymbol{\epsilon}[k]}_{\text{received Tx distortion}} + \mathbf{n}_\mu[k], \end{aligned} \quad (3b)$$

where $\mathbf{n}_\mu[k]$ is effective noise at user μ , which can be modeled as a zero-mean complex symmetric white Gaussian noise with $\mathcal{CN}(\mathbf{0}, N_0 \mathbf{I}_{N_{R_\mu}})$, where N_0 is the noise variance at the receiver. The transmit distortion on the receiver side of user μ at subcarrier k can be expressed by $\mathbf{H}_\mu[k] \boldsymbol{\epsilon}[k]$, which unfortunately correlates the total noise spatially at the receiver since the effective noise covariance matrix seen at the user side—ignoring the k -th index for brevity— $\mathbf{R}_\mu = \mathbf{H}_\mu \mathbf{R}_{\boldsymbol{\epsilon}\boldsymbol{\epsilon}} \mathbf{H}_\mu^H + N_0 \mathbf{I}_{N_{R_\mu}}$ where $\mathbf{R}_{\boldsymbol{\epsilon}\boldsymbol{\epsilon}} = \mathbb{E}\{\boldsymbol{\epsilon}\boldsymbol{\epsilon}^H\}$ is the transmit distortion covariance. Therefore, the impact of transmit distortion has unfortunately a well-known pernicious effect on the system-wide throughput, see, *e.g.*, [18]–[20], [35] and their references. To minimize the impact on the system throughput due to transmit distortion, we focus on reducing the transmitted $\boldsymbol{\epsilon}$ or/and received $\mathbf{H}_\mu \boldsymbol{\epsilon}$ distortion energy. For SU-MIMO received signal model, all the N_L spatial layers target a single user $\mu = 1$ having N_R receive antennas. Thus, the received signal model for both SU-MIMO and over all the receive antennas of N_U users in MU-MIMO is exactly same as $\mathbb{C}^{N_R \times 1} \ni \mathbf{Y}[:, k] = [\mathbf{Y}_1[:, k]; \dots; \mathbf{Y}_{N_U}[:, k]] \approx$

$\mathbf{H}[k] \mathbf{X}[:, k] + \mathbf{H}[k] \boldsymbol{\epsilon}[k] + \mathbf{n}[k]$. Hence, we will use the overall received signal model that is valid for both SU-MIMO and MU-MIMO.

B. Performance Metrics

We utilize three figures of merit: 1) PAPR and instantaneous PAPR (IPAPR), 2) inband distortions, and 3) OOB for the PAPR reduction algorithm design and its performance.

1) *PAPR and IPAPR*: The PAPR and IPAPR of the MIMO-OFDM signal in the time domain, per the j -th transmit antenna branch, are defined as $\text{PAPR}_j := \left\| \mathbf{F}^H (\mathbf{X}[j, :])^T \right\|_2^2 / \left\| \mathbf{F}^H (\mathbf{X}[j, :])^T \right\|_2^2$ and $\text{IPAPR}_j[n] := \left\| \left(\mathbf{F}^H (\mathbf{X}[j, :])^T \right)_n \right\|_2^2 / \left\| \mathbf{F}^H (\mathbf{X}[j, :])^T \right\|_2^2$, respectively, where $\mathbf{F}^H \in \mathbb{C}^{\ell K \times \ell K}$ is the IDFT matrix.

2) *Inband distortions*: The inband distortions are evaluated in terms of three EVM metrics², namely i) (unequalized) EVM at the transmitter, ii) predicted received EVM, and iii) estimated received EVM. Using (2) and (3), we define these three instantaneous performance and algorithm design metrics at subcarrier k for a given MIMO-OFDM symbol.

- (i) Transmit (unequalized) EVM: $\text{EVM}_{\text{Tx}}[k] := \left\| \bar{\mathbf{X}}[:, k] - \mathbf{X}[:, k] \right\|_2 / \left\| \mathbf{X}[:, k] \right\|_2 \approx \left\| \boldsymbol{\epsilon}[k] \right\|_2 / \left\| \mathbf{X}[:, k] \right\|_2$ represents the transmit signal distortion energy. For the performance evaluation, we assume that the average transmit signal power for each j -th transmit antenna branch $\mathbb{E} \left\{ \left\| \mathbf{X}[j, :] \right\|_2^2 \right\}$ is fixed, and the total signal energy per MIMO-OFDM symbol is the same before and after PAPR reduction.
- (ii) Predicted received EVM: $\text{EVM}_{\text{pred}}[k] := \left\| \mathbf{H}[k] (\bar{\mathbf{X}}[:, k] - \mathbf{X}[:, k]) \right\|_2 / \left(\left\| \mathbf{H}[k] \mathbf{X}[:, k] \right\|_2 \right)$ where $\{\mathbf{H}[k]\}$ is CSI acquired at the transmitter via the uplink channel for the user-specific transmission.
- (iii) Estimated received EVM per spatial layer after MIMO detection (with channel equalization): $\text{EVM}_{\text{est}}[l, k] := \left| \hat{\mathbf{S}}[l, k] - \mathbf{S}[l, k] \right| / \left| \mathbf{S}[l, k] \right|$, where $\hat{\mathbf{S}}[l, k] := \mathbf{G}[k] \mathbf{H}[k] \bar{\mathbf{X}}[:, k]$ corresponds to the estimated symbol for spatial layer l and subcarrier k with $\mathbf{G}[k] \in \mathbb{C}^{N_L \times N_T}$ equalizer at the receiver.

3) *Out-of-band emissions*: In this work, the OOB requirements are simply characterized by the amount of distortion energy on the unused subcarriers $k \in \mathcal{T}^\perp$ with respect to the useful data-carrying subcarriers $k \in \mathcal{T}$, which is referred to as the ACLR per j -th antenna and can mathematically be described as $\text{ACLR}_j := \left\| \bar{\mathbf{X}}[j, \mathcal{T}^\perp] \right\|_2^2 / \left\| \bar{\mathbf{X}}[j, \mathcal{T}] \right\|_2^2$. Note our ACLR definition in the description of optimization problem—posed in the subsequent section—can be seen as reciprocal to the 3GPP ACLR definition [24]. However, we interchangeably use both definitions but with the appropriate sign of the ACLR value.

²The EVM metric evaluation provides insightful and useful information on the link quality in terms of signal-to-noise ratio (SNR) seen at the receiver due to the aggregated digital and analogue hardware imperfections [43], [44]. Hence, in this study, we evaluate the inband performance in terms of proposed EVM metrics.

IV. PROPOSED EVM MITIGATION WITH PAPR AND ACLR CONSTRAINTS IN MIMO-OFDM

This section introduces proximal/operator splitting techniques, particularly, TOP-ADMM proposed recently in [35], that can tackle an appropriate optimization problem potentially yield computationally efficient algorithm for the large-scale optimization problem. In the sequel, we formulate a robust PAPR reduction problem that mitigates the predicted received EVM under channel estimates' uncertainty while targeting desired PAPR and ACLR levels. Subsequently, we formulate a robust problem amenable to the TOP-ADMM-type algorithms. Finally, we propose a computationally efficient TOP-ADMM-based algorithm and develop algorithms utilizing two popular BADMM [28] and DYS [32] techniques.

A. Efficient Proximal/Operator Splitting Algorithms

As discussed in Section II, we present some proximal/operator splitting techniques, notably TOP-ADMM, DYS, and BADMM that can render computationally efficient algorithms, typically using proximal operators, to solve a large-scale problem in a principled manner. We consider a generic problem,

$$\underset{\mathbf{x} \in \mathcal{X}}{\text{minimize}} \quad \sum_{m=1}^M f_m(\mathbf{x}) + g(\mathbf{x}) + \beta h(\mathbf{x}), \quad (4)$$

for some $M \geq 1$, where \mathcal{X} is a real/complex Euclidean space, $\{f_m(\cdot)\}$, $g(\cdot)$ and $h(\cdot)$ are closed, convex, and proper functions, and h is L -smooth (see Definition 1) with some scaling $\beta \in \mathbb{R}_{\geq 0}$. Foremost, we layout two useful definitions in the sequel to introduce proximal/operator splitting algorithms.

Definition 1 (L -smooth function [31], [45]). A differentiable function $f(\mathbf{z}) \in \mathbb{R}$, where $\mathbf{z} \in \mathbb{C}^n$, is L -smooth, i.e., has L -Lipschitz continuous gradient (for $L > 0$) if $\left\| \nabla f(\mathbf{z}_1) - \nabla f(\mathbf{z}_2) \right\| \leq L \left\| \mathbf{z}_1 - \mathbf{z}_2 \right\| \quad \forall \mathbf{z}_1, \mathbf{z}_2 \in \mathbb{C}^n$.

Definition 2 (Proximal mapping [27] [31]). Given a proper closed convex function $f : \text{dom}_f \mapsto (-\infty, +\infty]$, then the proximal mapping of f is the operator given by

$$\text{prox}_{\lambda f}(\mathbf{X}) = \arg \min_{\mathbf{Z} \in \text{dom}_f} \left\{ f(\mathbf{Z}) + \frac{1}{\beta \lambda} \left\| \mathbf{X} - \mathbf{Z} \right\|_F^2 \right\} \quad (5)$$

for any $\mathbf{X} \in \text{dom}_f$, where dom_f corresponds to the domain of a function f and $\lambda > 0$. If \mathbf{Z} is complex-valued or real-valued, $\beta = 1$ or $\beta = 2$, respectively.

Definition 3 (Proximal mapping of the indicator function [27] [31]). Let $f := \delta_C : \text{dom}_f \mapsto (-\infty, +\infty]$ be an indicator function (also known as characteristic function),

$$f(\mathbf{z}) = \delta_C(\mathbf{z}) := \begin{cases} 0, & \mathbf{z} \in C \\ +\infty, & \mathbf{z} \notin C, \end{cases} \quad (6)$$

then the proximal mapping of a given set $C \neq \emptyset$ is the orthogonal projection operator onto C , i.e.,

$$\text{prox}_{\lambda \delta_C}(\mathbf{z}) = \arg \min_{\mathbf{y} \in \text{dom}_f} \left\{ \delta_C(\mathbf{y}) + \frac{1}{\beta \lambda} \left\| \mathbf{z} - \mathbf{y} \right\|_2^2 \right\}$$

$$\equiv \arg \min_{\mathbf{y} \in \mathcal{C}} \left\{ \|\mathbf{z} - \mathbf{y}\|_2^2 \right\} = \mathbf{proj}_{\mathcal{C}}(\mathbf{z}).$$

In the subsequent sections, we present our proposed TOP-ADMM [35] generic algorithm, and briefly introduce DYS [32] and BADMM [28] algorithms.

1) *TOP-ADMM Algorithm [35]*: It is one of the generalized algorithms for the classical consensus ADMM—see details of ADMM and its applications in, *e.g.*, review paper [26]. This TOP-ADMM can be employed to solve many optimization problems³ that can be expressed as a composite problem such as (4)—which utilizes the gradient of L -smooth function h , unlike classical ADMM. The TOP-ADMM algorithm can be classified as a divide-and-conquer method, which decomposes a big optimization problem—difficult to solve in a composite form (7)—into smaller subproblems that are easy to solve.

Let us reformulate problem (4), without loss of generality, which has at least one solution, as

$$\begin{aligned} & \underset{\{\mathbf{x}_m \in \mathbb{C}^n\}, \mathbf{z} \in \mathbb{C}^n}{\text{minimize}} && \sum_{m=1}^M f_m(\mathbf{x}_m) + g(\mathbf{z}) + \beta h(\mathbf{z}) \\ & \text{subject to} && \mathbf{x}_m - \mathbf{z} = \mathbf{0}, \forall m = 1, \dots, M. \end{aligned} \quad (7)$$

We lay out the general definition of our TOP-ADMM method, which was introduced in [35].

Theorem 1 (TOP-ADMM). *Consider a problem given in (7) with at least one solution and a suitable step-size $\tau \in \mathbb{R}_{\geq 0}$. Assume subproblems (8a) and (8b) have solutions, and consider a relaxation/penalty parameter $\rho \in \mathbb{R}_{> 0}$ with some arbitrary initial $(\{\mathbf{x}_m^{(0)}\}, \mathbf{z}^{(0)}, \{\mathbf{y}_m^{(0)}\})$. Then*

$$\mathbf{x}_m^{(i+1)} = \arg \min_{\mathbf{x}_m} f_m(\mathbf{x}_m) + \rho \left\| \mathbf{x}_m - \mathbf{z}^{(i)} + \frac{\mathbf{y}_m^{(i)}}{\rho} \right\|_2^2 \quad \forall m \quad (8a)$$

$$\begin{aligned} \mathbf{z}^{(i+1)} = & \arg \min_{\mathbf{z}} g(\mathbf{z}) \\ & + \sum_{m=1}^M \rho \left\| \mathbf{x}_m^{(i+1)} - \mathbf{z} - \tau \nabla h(\mathbf{z}^{(i)}) + \frac{\mathbf{y}_m^{(i)}}{\rho} \right\|_2^2 \end{aligned} \quad (8b)$$

$$\mathbf{y}_m^{(i+1)} = \mathbf{y}_m^{(i)} + \rho \left(\mathbf{x}_m^{(i+1)} - \mathbf{z}^{(i+1)} \right) \quad \forall m = 1, \dots, M, \quad (8c)$$

at any limit point, converges to a Karush-Kuhn-Tucker (KKT) stationary point of (7).

Proof: We prove dual residual $\lim_{i \rightarrow +\infty} (\mathbf{z}^{(i+1)} - \mathbf{z}^{(i)}) = \mathbf{0}$ and primal residual $\lim_{i \rightarrow +\infty} (\mathbf{x}_m^{(i+1)} - \mathbf{z}^{(i+1)}) = \mathbf{0}$, $\forall m = 1, \dots, M$, hold under mild assumptions. Consequently, we establish the global convergence [46]. ■

Please observe that the classical consensus ADMM algorithm is a special case of our proposed TOP-ADMM algorithm when $h = 0$ in (7) or $\nabla h = 0$ in (8). Although classical consensus ADMM can solve many problems in signal processing for communications, it does not necessarily yield an implementation-friendly algorithm, particularly, if the

³For instance, see [35], where we applied TOP-ADMM to tackle a large-scale mask-compliant spectral precoding problem in the MIMO-OFDM-based wireless communication systems, particularly 5G NR.

proximal operator of L -smooth function h is inefficient to compute.

2) *DYS Algorithm [32]*: It tackles the subform of (4), *i.e.*,

$$\underset{\mathbf{x} \in \mathcal{X}}{\text{minimize}} \quad f_1(\mathbf{x}) + g(\mathbf{x}) + h(\mathbf{x}). \quad (9)$$

Theorem 2 (DYS). *Consider a step-size $\tau := (0, 2/L)$ with some arbitrary initial $\mathbf{z}^{(0)} \in \mathcal{X}$. Set $\varrho = 2 - (\tau L)/2$. Let $(\rho^{(i)})_{i \in \mathbb{N}}$ be a sequence in $[0, \varrho]$ such that $\sum_{i \in \mathbb{N}} \rho^{(i)} (\varrho - \rho^{(i)}) = +\infty$. Then, the sequence $\{\mathbf{x}^{(i+1)}\}$ generated by the following iterative scheme*

$$\mathbf{x}^{(i+1)} = \mathbf{prox}_{\tau f_1}(\mathbf{z}^{(i)}) \quad (10a)$$

$$\begin{aligned} \mathbf{z}^{(i+1)} = & \mathbf{z}^{(i)} + \rho^{(i)} \left[\mathbf{prox}_{\tau g}(2\mathbf{x}^{(i+1)} \right. \\ & \left. - \mathbf{z}^{(i)} - \tau \nabla h(\mathbf{x}^{(i+1)})) - \mathbf{x}^{(i+1)} \right], \end{aligned} \quad (10b)$$

converges to a solution of (9).

3) *BADMM Algorithm [28]*: Although this algorithm may seem to solve a two-operator problem, it utilizes the Bregman distance to linearize the L -smooth function h , and consequently solve the three-operator problem (9). We omit the details, but we refer the interested reader to [28, Section 2.1].

To this end, we formulate the problem that is amenable to the TOP-ADMM, DYS, and BADMM.

B. Proposed Problem Formulations

We propose a principled approach to mitigate (in CSI-aware mode under channel uncertainty) and/or minimize (in non-CSI-aware mode) signal distortion according to the appropriate conditions and/or requirements subject to the PAPR and ACLR constraints. Consequently, we first pose an optimization problem P0 that essentially minimizes the total transmit EVM over all the allocated subcarriers and transmit antennas, see (11a), subject to the three performance metrics introduced in Section III-B, namely nonconvex $\{\text{PAPR}_j\}$, see (11b), frequency-selective predicted received $\{\text{EVM}_{\text{pred}}[k]\}$, see (11c), and nonconvex $\{\text{ACLR}_j\}$, see (11d), constraints. Therefore, the optimization problem can mathematically be described as:

$$(\text{P0}) \quad \underset{\bar{\mathbf{X}} \in \mathbb{C}^{N_T \times \ell_K}}{\text{minimize}} \quad \|\bar{\mathbf{X}} - \mathbf{X}\|_F^2 \quad (11a)$$

$$\text{subject to} \quad \frac{\|\mathbf{F}^H \bar{\mathbf{X}}^T\|_2^2}{\|\mathbf{F}^H \mathbf{X}^T\|_2^2} \preceq \gamma_{\text{par}} \quad (11b)$$

$$\|\mathbf{H}[k] (\bar{\mathbf{X}} - \mathbf{X}) \mathbf{e}_k\|_2 \leq \epsilon_{\text{evm}}[k] \quad \forall k \in \mathcal{T} \quad (11c)$$

$$\frac{\|\bar{\mathbf{X}}[:, \mathcal{T}^\perp]\|_2^2}{\|\bar{\mathbf{X}}[:, \mathcal{T}]\|_2^2} \preceq \psi_{\text{aclr}}, \quad (11d)$$

where \preceq denotes element-wise inequality, and $\gamma_{\text{par}} \in \mathbb{R}^{N_T \times 1}$, $\epsilon_{\text{evm}}[k] \in \mathbb{R}$, and $\psi_{\text{aclr}} \in \mathbb{R}^{N_T \times 1}$ are predefined thresholds for the desired PAPR, the received EVM per k -th useful data-carrying subcarrier, and ACLR constraint, respectively. These predefined thresholds can be scalar, *i.e.*, the same values are used for all the antennas. Observe that this ACLR constraint is not shaping the spectrum such as the methods

described in [35], [38]. However, this constraint could ensure that the minimum 3GPP requirement of 45 dB [24] is met after some spectrum shaping, *e.g.*, $\psi_{\text{aclr}} = -50$ dB, see Section V. Furthermore, although in (11c) we have used a perfect channel estimate notation, subsequently, we develop a robust formulation that utilizes imperfect and/or incomplete channel estimates. Nevertheless, constraint (11c) can essentially exploit the excess spatial degrees-of-freedom to mitigate the transmit distortion at the receiver(s)—see Section V-B, particularly, Fig. 10 that shows that the (predicted/estimated) received EVM decreases with the increasing spatial degrees-of-freedom or number of base station transmit antennas. Notice that instead of constraining predicted received EVM in (11c), it is straightforward to constrain interlayer interference and the received distortion energy—cf. (2)—that is, replace the left hand of (11c) with $\|(\mathbf{H}[k] \bar{\mathbf{X}}[:, k] - \mathbf{S}[:, k])\|_2$. On the contrary, if the base station has no downlink channel knowledge, *e.g.*, catering to non-CSI-aware mode for the broadcast/control channel, then constraint (11c) can be omitted. In the sequel, we will reformulate this problem, which can easily adapt to CSI-aware and non-CSI-aware modes via suitable parameter settings.

Clearly, this problem P0 is nonconvex, in particular, due to the PAPR constraint (11b) and the ACLR constraint (11d), whereas objective (11a) and constraint (11c) are convex. One could convexify the PAPR constraint by resorting to peak clipping, *i.e.*, replacing the denominator in (11b), *i.e.*, $\|\mathbf{F}^H \bar{\mathbf{X}}^T\|_2^2$, with a fixed energy of the OFDM symbol, *i.e.*, $\mathbb{E} \left\{ \|\mathbf{F}^H \mathbf{X}^T\|_2^2 \right\}$, see, *e.g.*, [18]. However, such an approach would render a suboptimal solution. Therefore, one could employ a semidefinite relaxation to the PAPR constraint, see, *e.g.*, [20] to improve the accuracy of the solution at the cost of prohibitive computational complexity $\mathcal{O}((\ell K N_T)^{4.5})$. Similarly, one could convexify the ACLR constraint (11d) by replacing the denominator $\|\bar{\mathbf{X}}[:, \mathcal{T}]\|_2^2$ with $\|\mathbf{X}[:, \mathcal{T}]\|_2^2$. Thus, even if one convexifies problem P0 by employing fixed values to the denominators of PAPR and ACLR constraints, computing an optimal solution in real-time using off-the-shelf convex optimization solvers, typically employs interior-point methods, such as CVX [47] will result in prohibitively high computational complexity $\mathcal{O}((\ell K N_T)^{4.5})$. Thus, an interior-point-based algorithm is infeasible to deploy on current state-of-the-art radio base stations. Hence, we seek a computationally efficient algorithm tackling the proposed problem that can be employed in realistic radio systems.

Toward the goal to develop efficient algorithms, unfortunately proposed problem P0 is not amenable to first-order optimization methods, notably operator/proximal splitting—see Section II-D and Section IV-A. Hence, we must reformulate the problem P0. For the problem reformulation, we now define two sets:

$$\begin{aligned} \mathcal{P} &:= \left\{ \bar{\mathbf{X}} : \|\bar{\mathbf{T}}\|_\infty \preceq \gamma_{\text{par}}^{\frac{1}{2}} \|\bar{\mathbf{T}}\|_2; \bar{\mathbf{T}} = \mathbf{F}^H \bar{\mathbf{X}}^T \right\} \\ &\equiv \left\{ \bar{\mathbf{X}} : \|\bar{\mathbf{T}} \mathbf{e}_j\|_\infty^2 \leq \gamma_{\text{par}} \|\bar{\mathbf{T}} \mathbf{e}_j\|_2^2; \bar{\mathbf{T}} = \mathbf{F}^H \bar{\mathbf{X}}^T; j = 1, \dots, N_T \right\} \end{aligned} \quad (12)$$

$$\begin{aligned} \mathcal{U} &:= \left\{ \bar{\mathbf{X}} : \|\bar{\mathbf{X}}[:, \mathcal{T}^\perp]\|_2 \preceq \psi_{\text{aclr}}^{\frac{1}{2}} \|\bar{\mathbf{X}}[:, \mathcal{T}]\|_2 \right\} \\ &\equiv \left\{ \bar{\mathbf{X}} : \|(\bar{\mathbf{X}}[:, \mathcal{T}^\perp]) \mathbf{e}_j^T\|_2^2 \leq \psi_{\text{aclr}} \|(\bar{\mathbf{X}}[:, \mathcal{T}]) \mathbf{e}_j^T\|_2^2; \forall j \right\} \end{aligned} \quad (13)$$

corresponding to the nonconvex PAPR (11b) and ACLR (11d) constraints, respectively. Subsequently, we use an indicator function to these sets \mathcal{P} and \mathcal{U} , *i.e.*, $\delta_{\mathcal{P}}(\bar{\mathbf{X}})$ and $\delta_{\mathcal{U}}(\bar{\mathbf{X}})$, where the indicator function definition to any set \mathcal{C} is given in (6). Furthermore, we define $h_{\text{TxEVM}}(\bar{\mathbf{X}}) := \|\bar{\mathbf{X}} - \mathbf{X}\|_F^2$. Consequently, using these definitions, we can reformulate an equivalent problem to P0, without loss of generality, as

$$(P1) \quad \underset{\bar{\mathbf{X}} \in \mathbb{C}^{N_T \times \ell K}}{\text{minimize}} \quad h_{\text{TxEVM}}(\bar{\mathbf{X}}) + \delta_{\mathcal{P}}(\bar{\mathbf{X}}) + \delta_{\mathcal{U}}(\bar{\mathbf{X}}) \quad (14a)$$

$$\text{subject to} \quad \|\mathbf{H}[k] (\bar{\mathbf{X}} - \mathbf{X}) \mathbf{e}_k\|_2^2 \leq \epsilon_{\text{evm}}^2[k] \quad \forall k \in \mathcal{T}. \quad (14b)$$

Clearly, problem P1 is equally hard to solve as P0 because of nonconvexity of indicator functions to nonconvex sets \mathcal{P} and \mathcal{U} . Question remains whether there are any possible (approximate) techniques to solve P1. Unfortunately, the answer is still negative unless there is some reformulation.

Before we progress further on tackling nonconvex problem P0/P1, let us express convexified problem P0/P1 in an unconstrained form:

(Convexified: P2)

$$\underset{\bar{\mathbf{X}} \in \mathbb{C}^{N_T \times \ell K}}{\text{minimize}} \quad h_{\text{TxEVM}}(\bar{\mathbf{X}}) + \delta_{\mathcal{P}^{(0)}}(\bar{\mathbf{X}}) + \delta_{\mathcal{U}^{(0)}}(\bar{\mathbf{X}}) + \delta_{\mathcal{E}}(\bar{\mathbf{X}}), \quad (15)$$

where convexified PAPR constraint set reads

$$\mathcal{P}^{(0)} := \left\{ \bar{\mathbf{X}} : \|\bar{\mathbf{T}}\|_\infty \preceq \sqrt{\gamma_{\text{par}}} \|\bar{\mathbf{T}}\|_2; \bar{\mathbf{T}} = \mathbf{F}^H \bar{\mathbf{X}}^T; \mathbf{T} = \mathbf{F}^H \mathbf{X}^T \right\}$$

and convexified ACLR constraint set is

$$\mathcal{U}^{(0)} := \left\{ \bar{\mathbf{X}} : \|\bar{\mathbf{X}}[:, \mathcal{T}^\perp]\|_2 \preceq \sqrt{\psi_{\text{aclr}}} \|\bar{\mathbf{X}}[:, \mathcal{T}]\|_2 \right\},$$

i.e., the respective denominators are fixed as discussed previously. The convex set corresponding to the predicted received EVM can be denoted by $\mathcal{E} := \left\{ \bar{\mathbf{X}} : \|\mathbf{H}[k] (\bar{\mathbf{X}} - \mathbf{X}) \mathbf{e}_k\|_2^2 \leq \epsilon_{\text{evm}}^2[k] \quad \forall k \in \mathcal{T} \right\}$.

Although problem P2 is convex, employing off-the-shelf solvers like CVX [47] is not easible for a realistic radio systems due to prohibitive high computational complexity. Hence, developing a computationally efficient algorithm is challenging using any (first-order) proximal splitting algorithm for problem P1/P2, notably and unfortunately due to the computation of proximal operator for $\delta_{\mathcal{E}}(\bar{\mathbf{X}})$, *i.e.*, an orthogonal projection operator on an ellipsoid having rank ≥ 1 as it involves eigenvalue decomposition—see, *e.g.* [35, Theorem 4] and their references. In other words, the orthogonal projection operator of such an ellipsoid for the predicted received EVM is computationally expensive. Although the orthogonal projection operators corresponding to the nonconvex ACLR and PAPR constraints are still notoriously hard, we will propose later in the subsequent sections how to possibly tackle these nonconvex constraints. Before proceeding further on attacking predicted received EVM constraint, let us formulate a robust version of predicted received EVM against channel uncertainty if channel estimates are available.

Problem P1 Reformulation for Robust Mitigation of Distor-

tion: Dropping subcarrier index k , let the channel estimation error model be described by $\mathbf{H} := \widehat{\mathbf{H}} + \Delta\mathbf{H}$, where \mathbf{H} , $\widehat{\mathbf{H}}$, and $\Delta\mathbf{H}$ denote true, estimated, and error, respectively. Additionally, let the error at subcarrier k be denoted by $\Delta\mathbf{X} := (\overline{\mathbf{X}}[:,k] - \mathbf{X}[:,k])$. Furthermore, for simplicity, we assume that $\Delta\mathbf{H}$ takes values from the bounded set $\{\|\Delta\mathbf{H}\|_F^2 \leq \sigma_{ce}^2\}$, where $\sigma_{ce}^2 > 0$ describes the channel uncertainty that is assumed to be known to the transmitter. Applying the triangle inequality followed by the Cauchy-Schwarz inequality to (11c)/(14b), we have

$$\begin{aligned} \|\mathbf{H}\Delta\mathbf{X}\|_2^2 &= \|(\widehat{\mathbf{H}} + \Delta\mathbf{H})\Delta\mathbf{X}\|_2^2 \\ &\leq \|\widehat{\mathbf{H}}\Delta\mathbf{X}\|_2^2 + \|\Delta\mathbf{H}\Delta\mathbf{X}\|_2^2 \\ &\leq \Delta\mathbf{X}^H (\widehat{\mathbf{H}}^H \widehat{\mathbf{H}} + \sigma_{ce}^2 \mathbf{I}) \Delta\mathbf{X}. \end{aligned} \quad (16)$$

Using the inequality (16) in the constraint (11c)/(14b), the channel estimation error-aware constraint is guaranteed if $\|Q^{1/2}[k](\overline{\mathbf{X}} - \mathbf{X})\mathbf{e}_k\|_2 \leq \epsilon_{\text{evm}}[k]$, where matrix \mathbf{Q} is defined as

$$\mathbb{C}^{N_T \times N_T} \ni \mathbf{Q}[k] := (\widehat{\mathbf{H}}[k]^H \widehat{\mathbf{H}}[k] + \nu \mathbf{I}_{N_T}), \quad (17)$$

where ν is a user-defined parameter to regularize the Gram matrix under channel estimation error. However, the ν parameter does not have to be the same as the channel estimation error variance σ_{ce}^2 —see Fig. 11, which shows the estimated received EVM metric against channel estimation error variance for a fixed ν .

To achieve our computationally efficient algorithms for our proposed problem, let us further reformulate the problem P1 under channel uncertainty by forming the Lagrangian such that we have

$$\begin{aligned} L_{P1}(\overline{\mathbf{X}}, \{\lambda_k\}) &:= h_{\text{TxEVM}}(\overline{\mathbf{X}}) + \delta_{\mathcal{P}}(\overline{\mathbf{X}}) + \delta_{\mathcal{U}}(\overline{\mathbf{X}}) \\ &\quad + \sum_{k \in \mathcal{T}} \lambda_k \left(\|Q^{1/2}[k](\overline{\mathbf{X}} - \mathbf{X})\mathbf{e}_k\|_2^2 - \epsilon_{\text{evm}}^2[k] \right). \end{aligned}$$

As we know from the Lagrange duality [23], the primal problem P1 can equivalently be expressed as

$$\underset{\overline{\mathbf{X}}}{\text{minimize}} \quad \sup_{\{\lambda_k\}} L_{P1}(\overline{\mathbf{X}}, \{\lambda_k\}).$$

It is well-known that the dual function $d(\{\lambda_k\}) := \inf_{\overline{\mathbf{X}}} L_{P1}(\overline{\mathbf{X}}, \{\lambda_k\})$ is a concave function due to pointwise infimum of affine functions of λ_k , even if the primal problem is nonconvex. Moreover, for the inequality constraint, the Lagrange multipliers are nonnegative $\lambda_k \in \mathbb{R}_{\geq 0}$. Unfortunately, computing a dual function for problem P1 is not trivial, which yields a lower bound on the optimal primal value. Therefore, toward the goal to develop implementation-friendly algorithms, let us assume that we have access to near/sub-optimal Lagrange multipliers $\lambda_k^* \in \mathbb{R}_{\geq 0}$. Hence, we now reformulate problem P1 that is robust against channel uncertainty and avoids costly orthogonal projections onto ellipsoids corresponding to predicted received EVM even though the problem is still nonconvex:

$$\begin{aligned} &\underset{\overline{\mathbf{X}} \in \mathbb{C}^{N_T \times \ell K}}{\text{minimize}} \{L_{P1}(\overline{\mathbf{X}}, \{\lambda_k^*\})\} \\ &= h_{\text{TxEVM}}(\overline{\mathbf{X}}) + \sum_{k \in \mathcal{T}} \lambda_k^* \left\| Q^{1/2}[k](\overline{\mathbf{X}} - \mathbf{X})\mathbf{e}_k \right\|_2^2 \end{aligned}$$

$$+ \delta_{\mathcal{P}}(\overline{\mathbf{X}}) + \delta_{\mathcal{U}}(\overline{\mathbf{X}}) \}. \quad (18)$$

We now absorb $\lambda_k = \lambda_k^*$ in $\mathbf{Q}[k]$ and offer a trade-off between h_{TxEVM} and the predicted received EVM with a user-defined parameter $\zeta \in \mathbb{R}_{\geq 0}$. Consequently, we succinctly represent the above problem as

$$(\text{P3}) \quad \underset{\overline{\mathbf{X}} \in \mathbb{C}^{N_T \times \ell K}}{\text{minimize}} \quad \delta_{\mathcal{P}}(\overline{\mathbf{X}}) + \delta_{\mathcal{U}}(\overline{\mathbf{X}}) + h(\overline{\mathbf{X}}), \quad (19)$$

where

$$h(\overline{\mathbf{X}}) := \sum_{k \in \mathcal{T}} \left\| Q^{1/2}[k](\overline{\mathbf{X}} - \mathbf{X})\mathbf{e}_k \right\|_2^2 + \zeta h_{\text{TxEVM}}(\overline{\mathbf{X}}) \quad (20)$$

is a differentiable function, the gradient of which is

$$\nabla h(\overline{\mathbf{X}}) = \sum_{k \in \mathcal{T}} \mathbf{Q}[k](\overline{\mathbf{X}} - \mathbf{X})\mathbf{e}_k \mathbf{e}_k^T + \zeta(\overline{\mathbf{X}} - \mathbf{X}). \quad (21)$$

If ζ is a large value, then EVM at the transmitter will be minimized more than the predicted received EVM. Observe that when the base station has no downlink channel knowledge, e.g., for broadcast channels, then one possibility is $\mathbf{Q}[k] = \lambda_k \mathbf{I}_{N_T}$ with $\lambda_k \in \mathbb{R}_{\geq 0}$ and other possibilities can be explored in future work. Observe that one could argue that it is not easy to find optimal dual variables λ_k^* . Therefore, alternatively, one can envisage to minimize the maximum over all the predicted received EVM, i.e., $\max \left\{ \left\| Q^{1/2}[k](\overline{\mathbf{X}} - \mathbf{X})\mathbf{e}_k \right\|_2^2 \right\}$ —reminiscent of infinite norm. Unfortunately, this approach is equally implementation unfriendly as minimizing peaks (or convexified PAPR), i.e., minimizing the infinite norm. Thus, we do not pursue this approach further in this work.

Before we attack on the nonconvexity of problem P3, we convexify P3 similar to (15):

$$(\text{Convexified: P4})$$

$$\underset{\overline{\mathbf{X}} \in \mathbb{C}^{N_T \times \ell K}}{\text{minimize}} \quad \delta_{\mathcal{P}^{(0)}}(\overline{\mathbf{X}}) + \delta_{\mathcal{U}^{(0)}}(\overline{\mathbf{X}}) + h(\overline{\mathbf{X}}). \quad (22)$$

Reiterating, although this convex problem P4 can be solved by any off-the-shelf solvers such as CVX [47], clearly, a general purpose solver is infeasible in realistic radio systems. Hence, we forage for computationally efficient algorithms to solve large-scale problem P3 and P4.

C. Efficient Solution of P3 Utilizing TOP-ADMM-type Algorithms

In this section, we develop three implementation-friendly algorithms utilizing TOP-ADMM, DYS, and BADMM techniques described in Section IV-A, which solve problem P3 by invoking our proposed conjecture. Naturally, these designed algorithms inherently tackle problem P4 as a special case.

In general, the considered proximal/operator splitting techniques, described in Section IV-A, need to compute the proximal operators of indicator functions $\delta_{\mathcal{P}}$ and $\delta_{\mathcal{U}}$ to nonconvex sets, i.e., orthogonal projections onto the respective nonconvex sets—see Definition 3. Unfortunately, no (efficient) projection operators $\text{proj}_{\mathcal{P}}$ and $\text{proj}_{\mathcal{U}}$ are known for the nonconvex PAPR and ACLR sets, i.e., \mathcal{P} and \mathcal{U} , respectively. On the contrary, for the convexified problem P4, the orthogonal projection operator $\text{proj}_{\mathcal{P}^{(0)}}$ for the convexified PAPR constraint set $\mathcal{P}^{(0)}$ is l_{∞} -norm ball for each transmit antenna, which is provided below in Proposition 1. Furthermore, the orthogonal projection operator $\text{proj}_{\mathcal{U}^{(0)}}$ for the convexified

ACLR constraint set $\mathcal{U}^{(0)}$ is l_2 -norm ball for each transmit antenna, which is given below in Proposition 2.

Proposition 1 (Proj onto the l_∞ -norm ball). *Let $\mathcal{C} = \{\mathbf{x} \in \mathbb{C}^{K \times 1} : \|\mathbf{x}\|_\infty - r \leq 0\}$, where $r \in \mathbb{R}_{\geq 0}$, then the orthogonal projection operator is $\text{proj}_{\mathcal{C}}(\mathbf{x}) = \left(\left(\frac{x[k]}{|x[k]|} \right) \min\{|x[k]|, r\} \right)_{1 \leq k \leq K}$.*

Proof: Invoking the Moreau decomposition theorem [31, Section 6.6] and using the l_1 -norm proximal operator result [31, Example 6.8], the proof follows after the rearrangement. ■

Proposition 2 (Proj onto the l_2 -norm ball [31, Lemma 6.26]). *Let $E \subseteq \mathbb{C}^{p \times 1}$ and $E \neq \emptyset$ be given by $E := \mathcal{B}_{\|\cdot\|_2}[\mathbf{c}, r] = \{\mathbf{x} \in \mathbb{C}^{p \times 1} : \|\mathbf{x} - \mathbf{c}\|_2 \leq r\}$, then the orthogonal projection operator for the l_2 -norm ball, i.e., $\mathcal{B}_{\|\cdot\|_2}[\mathbf{c}, r]$ with a given center \mathbf{c} and the radius r , is $\text{proj}_{\mathcal{B}_{\|\cdot\|_2}[\mathbf{c}, r]}(\mathbf{x}) = \mathbf{c} + \left(\frac{r}{\max\{\|\mathbf{x} - \mathbf{c}\|_2, r\}} \right) (\mathbf{x} - \mathbf{c})$.*

Toward the goal to develop efficient algorithms utilizing TOP-ADMM-type techniques for nonconvex problem P3 (and inherently for P4 as a special case), we solve the appropriate subproblems at iteration $(i+1)$ by replacing the nonconvex constraint sets (12) and (13) with the following convex but employing generated sequence $\bar{\mathbf{X}}^{(i)}$ of previous iteration i for PAPR and ACLR constraint sets:

$$\begin{aligned} \mathcal{P}^{(i)} &:= \left\{ \bar{\mathbf{X}} : \|\bar{\mathbf{T}}\|_\infty \leq \sqrt{\gamma_{\text{par}}} \|\bar{\mathbf{T}}^{(i)}\|_2; \right. \\ &\quad \left. \bar{\mathbf{T}} = \mathbf{F}^H \bar{\mathbf{X}}^T; \bar{\mathbf{T}}^{(i)} = \mathbf{F}^H \left(\bar{\mathbf{X}}^{(i)} \right)^T \right\}, \\ \mathcal{U}^{(i)} &:= \left\{ \bar{\mathbf{X}} : \|\bar{\mathbf{X}}[:, \mathcal{T}^\perp]\|_2 \leq \psi_{\text{aclr}}^{\frac{1}{2}} \|\bar{\mathbf{X}}^{(i)}[:, \mathcal{T}]\|_2 \right\}. \end{aligned}$$

Theorem 1 establishes the global convergence of TOP-ADMM for the general convex problem. However, based on extensive numerical evidence, we conjecture that the asymptotically vanishing property of the (dual/primal) residual errors of TOP-ADMM holds for the nonconvex problem P3 with iteration-dependent sets—see Fig. 6–Fig. 9. Consequently, under this conjecture, the proposed TOP-ADMM algorithm satisfies the KKT optimality conditions of nonconvex problem P3—see Appendix A. Additionally, this optimality condition implies that $\lim_{i \rightarrow \infty} \mathcal{P}^{(i)} = \mathcal{P}$ and $\lim_{i \rightarrow \infty} \mathcal{U}^{(i)} = \mathcal{U}$. Therefore, we argue that a KKT point for nonconvex P3 is not worse than a KKT point of convex P4 by applying TOP-ADMM-type techniques. Noticeably, in Fig. 5 and Fig. 12, the iteration-dependent set renders a better solution compared to the fixed set for the considered test cases. However, proving the conjecture⁴ is the topic of future research.

⁴During the revision process, we came across [48] and its references, which evidently employs similar techniques within the “majorization-minimization” framework to approximate the nonconvex constraint set for a difference of convex functions, i.e., $f(x) - g(x) \leq 0$.

Algorithm 1 TOP-ADMM-based PAPR Reduction for P3/P4

Initialization: $\bar{\mathbf{X}}^{(0)}, \bar{\mathbf{Z}}^{(0)}, \boldsymbol{\Lambda}^{(0)} \in \mathbb{C}^{N_T \times \ell K}$, $\tau \in \mathbb{R}$; $\{\mathbf{Q}[k] \in \mathbb{C}^{N_T \times N_T}\}$;
 $\rho \in \mathbb{R}_{>0}$

Output(s): $\bar{\mathbf{X}}^{(\cdot)} \in \mathbb{C}^{N_T \times \ell K}$ or $\bar{\mathbf{Z}}^{(\cdot)} \in \mathbb{C}^{N_T \times \ell K}$

1: **for** $i = 0, 1, \dots$ **do**

$$\bar{\mathbf{X}}^{(i+1)} := \text{proj}_{\mathcal{U}^{(i)}} \left(\bar{\mathbf{Z}}^{(i)} - \frac{\boldsymbol{\Lambda}^{(i)}}{\rho} \right) \quad (23a)$$

$$\begin{aligned} \bar{\mathbf{Z}}^{(i+1)} &:= \text{proj}_{\mathcal{P}^{(i)}} \left(\bar{\mathbf{X}}^{(i+1)} - \tau \nabla h(\bar{\mathbf{Z}}^{(i)}) + \frac{\boldsymbol{\Lambda}^{(i)}}{\rho} \right) \\ &\equiv \left[\mathbf{F} \text{proj}_{\mathcal{P}^{(i)}} \left(\mathbf{F}^H \left(\bar{\mathbf{X}}^{(i+1)} - \tau \nabla h(\bar{\mathbf{Z}}^{(i)}) + \frac{\boldsymbol{\Lambda}^{(i)}}{\rho} \right)^T \right) \right]^T \end{aligned} \quad (23b)$$

$$\boldsymbol{\Lambda}^{(i+1)} := \boldsymbol{\Lambda}^{(i)} + \rho \left(\bar{\mathbf{X}}^{(i+1)} - \bar{\mathbf{Z}}^{(i+1)} \right) \quad (23c)$$

2: **end for**

1) *TOP-ADMM-Based Algorithm for P3/P4:* For the brevity of the algorithm description, we redefine the PAPR set $\mathcal{P}_T^{(i)} := \left\{ \bar{\mathbf{T}} : \|\bar{\mathbf{T}}\|_\infty \leq \sqrt{\gamma_{\text{par}}} \|\bar{\mathbf{T}}^{(i)}\|_2 \right\}$ and apply TOP-ADMM method (8) to tackle P3/P4 by setting $M = 1$, $f_1 = \delta_{\mathcal{U}^{(i)}}$, $g = \delta_{\mathcal{P}^{(i)}}$, $\bar{\mathbf{X}} = \mathbf{x}_1$, $\bar{\mathbf{Z}} = \mathbf{z}$, $\boldsymbol{\Lambda} = \mathbf{y}_1$. The resulting TOP-ADMM-based algorithm for P3/P4 is given in Algorithm 1. The gradient ∇h is given by (21). Observe that both primal updates, i.e., (23a) and (23b), are easy to solve and have closed-form solutions. For the $\bar{\mathbf{X}}^{(i+1)}$ update in (23a)—corresponding to $\text{proj}_{\mathcal{U}^{(i)}}$ —we apply Proposition 2 with center $\mathbf{C} = \mathbf{0}$ and radius $r = \sqrt{\psi_{\text{aclr}}} \|\bar{\mathbf{X}}^{(i)}[:, \mathcal{T}]\|_2$. Subsequently, we invoke Proposition 3 for the $\bar{\mathbf{X}}^{(i+1)}$ and $\bar{\mathbf{Z}}^{(i+1)}$ updates in (23a) and (23b), respectively, such that the updates are performed independently for each transmit antenna. Consequently, the orthogonal projection in (23a), i.e., $\text{proj}_{\mathcal{U}^{(i)}}$, corresponding to the ACLR constraint for each transmit antenna, is given by Proposition 2. The orthogonal projection in (23b), i.e., $\text{proj}_{\mathcal{P}^{(i)}}$, corresponding to the PAPR constraint per transmit antenna branch is given by Proposition 1. Moreover, (23b) update exploits the proximal operator property given in Proposition 4. Notice that to solve P4, the sets for both PAPR and ACLR are not iteration dependent, i.e., we set $\text{proj}_{\mathcal{U}^{(i)}} = \text{proj}_{\mathcal{U}^{(0)}}$ and $\text{proj}_{\mathcal{P}^{(i)}} = \text{proj}_{\mathcal{P}^{(0)}}$ for all $i \geq 0$.

Proposition 3 (Separation theorem for proximal operators [27], [31]). *If a function $f(\mathbf{X}) = \sum_{k=1}^n f_i(\mathbf{x}_k)$ is separable across the variables column-wise $\mathbf{X} = [\mathbf{x}_1, \dots, \mathbf{x}_n]$ and row-wise $\mathbf{X} = [\mathbf{x}_1; \dots; \mathbf{x}_{N_T}]$, then the respective prox operators are as $\text{prox}_f(\mathbf{X}) = [\text{prox}_{f_1}(\mathbf{x}_1), \dots, \text{prox}_{f_n}(\mathbf{x}_n)]$ and $\text{prox}_f(\mathbf{X}) = [\text{prox}_{f_1}(\mathbf{x}_1); \dots; \text{prox}_{f_{N_T}}(\mathbf{x}_{N_T})]$, respectively.*

Proposition 4 (Prox map for composition with an affine mapping [31, Theorem 6.15]). *Let $g : \mathbb{C}^{m \times 1} \mapsto (-\infty, +\infty]$ be a closed proper convex, and $f(\mathbf{x}) = g(\mathcal{A}(\mathbf{x}) + \mathbf{b})$, where $\mathbf{b} \in \mathbb{C}^{m \times 1}$ and $\mathcal{A} : \mathcal{X} \mapsto \mathbb{C}^{m \times 1}$ satisfying $\mathcal{A} \circ \mathcal{A}^H = \nu \mathbf{I}$ where $\nu \in \mathbb{R}_{>0}$, then for any $\mathbf{x} \in \mathbb{C}^{n \times 1}$ $\text{prox}_f(\mathbf{x}) = \mathbf{x} + \frac{1}{\lambda} \mathcal{A}^H(\text{prox}_{\lambda g}(\mathcal{A}(\mathbf{x}) + \mathbf{b}) - \mathcal{A}(\mathbf{x}) - \mathbf{b})$.*

Algorithm 2 Bregman ADMM-based PAPR Reduction for P3/P4

Initialization: $\bar{\mathbf{X}}^{(0)}, \bar{\mathbf{Z}}^{(0)}, \mathbf{\Lambda}^{(0)} \in \mathbb{C}^{N_T \times \ell K}$; $\{\mathbf{Q}[k] \in \mathbb{C}^{N_T \times N_T}\}$;
 $\rho, \rho_x, \rho_z, \tau \in \mathbb{R}_{>0}$

Output(s): $\bar{\mathbf{X}}^{(\cdot)} \in \mathbb{C}^{N_T \times \ell K}$ or $\bar{\mathbf{Z}}^{(\cdot)} \in \mathbb{C}^{N_T \times \ell K}$

1: **for** $i = 0, 1, \dots$ **do**

$$\mathbf{U} := \rho_x \bar{\mathbf{X}}^{(i)} - \nabla h(\bar{\mathbf{X}}^{(i)}) + \rho \left(\bar{\mathbf{Z}}^{(i)} - \frac{\mathbf{\Lambda}^{(i)}}{\rho} \right) \quad (24a)$$

$$\bar{\mathbf{X}}^{(i+1)} := \text{proj}_{\mathcal{U}^{(i)}} \left(\frac{\mathbf{U}}{(\rho_x + \rho_z)} \right) \quad (24b)$$

$$\mathbf{V} := \frac{1}{(\rho_z + \rho)} \left(\rho_z \bar{\mathbf{Z}}^{(i)} - \nabla h(\bar{\mathbf{Z}}^{(i)}) + \rho \left(\bar{\mathbf{X}}^{(i+1)} + \frac{\mathbf{\Lambda}^{(i)}}{\rho} \right) \right) \quad (24c)$$

$$\bar{\mathbf{Z}}^{(i+1)} := \left[\mathbf{F} \text{proj}_{\mathcal{P}_T^{(i)}} \left(\mathbf{F}^H \mathbf{V} \right) \right]^T \quad (24d)$$

$$\mathbf{\Lambda}^{(i+1)} := \mathbf{\Lambda}^{(i)} + \tau \left(\bar{\mathbf{X}}^{(i+1)} - \bar{\mathbf{Z}}^{(i+1)} \right) \quad (24e)$$

2: **end for**

To benchmark our proposed Algorithm 1 using TOP-ADMM against state-of-the-art algorithms, we next present two algorithms applying BADMM and DYS methods to solve P3/P4. Recall, to solve P4, the sets for both PAPR and ACLR are iteration independent, *i.e.*, $\text{proj}_{\mathcal{U}^{(i)}} = \text{proj}_{\mathcal{U}^{(0)}}$ and $\text{proj}_{\mathcal{P}^{(i)}} = \text{proj}_{\mathcal{P}^{(0)}}$ for all the iterations $i \geq 0$.

D. Bregman ADMM (BADMM) Algorithm

We develop first reference algorithm using BADMM [28], cf. Section IV-A3, for benchmarking purposes to solve P3/P4, whose recipe is presented in Algorithm 2—see [1] for additional algorithmic details. The operators $\text{proj}_{\mathcal{P}^{(i)}}$, $\text{proj}_{\mathcal{U}^{(i)}}$, and ∇h can be computed as described for the TOP-ADMM algorithm.

E. Davis-Yin Splitting (DYS) Algorithm

Lastly, we also designed another reference algorithm for benchmarking purposes using DYS [32], cf. Section IV-A2 tackling P3/P4—the recipe is given in Algorithm 3. Similarly, the projection operators $\text{proj}_{\mathcal{P}^{(i)}}$ and $\text{proj}_{\mathcal{U}^{(i)}}$, and gradient ∇h are same as described for the TOP-ADMM algorithm.

F. Computational Complexity Analysis

We compare the run-time computational complexities of our proposed TOP-ADMM-type algorithms with two prior arts, namely semidefinite relaxation-based [20] and Bao et al. [19]. Let $K_D := |\mathcal{T}|$ denote the number of useful data-carrying subcarriers. Consequently, let $K_C := |\mathcal{T}^\perp|$ such that $K = K_D + K_C$.

Common processing of TOP-ADMM-type algorithms: the major computational complexity of all the three presented algorithms stem from IDFT and DFT operations, and gradient ∇h . The cost of IDFT or DFT is typically $\mathcal{O}(\ell K \log(\ell K))$ per iteration. Additionally, the worst-case cost in computing the gradient ∇h (21) is $\mathcal{O}(K_D N_T^2)$. Observe that the computation of $\{\mathbf{Q}[k]\}$ matrices is required only once per subcarrier, which is $\mathcal{O}(K_D N_R N_T^2)$. The computational cost of orthogonal projection operators is relatively

Algorithm 3 DYS-based PAPR Reduction for P3/P4

Initialization: $\bar{\mathbf{X}}^{(0)}, \bar{\mathbf{Z}}^{(0)}, \mathbf{\Lambda}^{(0)} \in \mathbb{C}^{N_T \times \ell K}$; $\{\mathbf{Q}[k] \in \mathbb{C}^{N_T \times N_T}\}$; $\tau, \mu \in \mathbb{R}_{\geq 0}$

Output(s): $\bar{\mathbf{X}}^{(\cdot)} \in \mathbb{C}^{N_T \times \ell K}$ or $\bar{\mathbf{Z}}^{(\cdot)} \in \mathbb{C}^{N_T \times \ell K}$

1: **for** $i = 0, 1, \dots$ **do**

$$\bar{\mathbf{X}}^{(i+1)} := \text{proj}_{\mathcal{U}^{(i)}} \left(\mathbf{\Lambda}^{(i)} \right) \quad (25a)$$

$$\bar{\mathbf{Z}}^{(i+1)} := \left[\mathbf{F} \text{proj}_{\mathcal{P}_T^{(i)}} \left(\mathbf{F}^H \left(2\bar{\mathbf{X}}^{(i+1)} - \mathbf{\Lambda}^{(i)} - \tau \nabla h(\bar{\mathbf{X}}^{(i+1)}) \right) \right) \right]^T \quad (25b)$$

$$\mathbf{\Lambda}^{(i+1)} := \mathbf{\Lambda}^{(i)} + \mu \left(\bar{\mathbf{Z}}^{(i+1)} - \bar{\mathbf{X}}^{(i+1)} \right) \quad (25c)$$

2: **end for**

low compared to IDFT/DFT operation. Hence, the overall complexity of the proposed TOP-ADMM-type algorithms is $\mathcal{O}((N_T \ell K \log(\ell K)) + K_D N_T^2)$. Table I summarizes and compares the complexity of the proposed schemes with three prior arts. Clearly, the semidefinite relaxation-based method [20] is impractical to deploy on the current state-of-the-art chipsets due to prohibitive complexity cost compared to the proposed first-order-based approaches. Moreover, another drawback of the prior art [19] is the need to resort to iterative numerical optimization, *e.g.*, a bisection method. This can be used to solve the proximal operator for the infinite norm—referred to as PROXINF in [19]—which has a complexity of $\mathcal{O}(I' N_T \ell K)$, where I' denotes the number of iterations. Nevertheless, the complexity of the prior art, Bao et al. [19], is similar to our TOP-ADMM-type schemes.

V. SIMULATION RESULTS

We present the performance of the proposed algorithms and benchmark their performance with the prior art [19] utilizing a 5G NR-like simulator for physical downlink shared channel (PDSCH). We analyze the PAPR reduction performance in terms of three figures of merit briefly described in Section III-B.

A. Simulation Assumptions and Parameters

The general simulation assumptions and parameters are given in Table II, and 3GPP NR wideband (average) EVM requirements (after equalization⁵) for each respective modulation alphabet are shown in Table III. Furthermore, we assume a base station supporting sub-6 GHz, *e.g.*, frequency ranges between 410 MHz and 7.125 GHz, referred to as FR1 in 5G NR [24, Section 5.1]. Note that we do not model any additional radio hardware impairments at the transmitter and/or receiver besides the distortion generated at the transmitter by the considered PAPR reduction methods, if enabled.

In Fig. 2, we illustrate channel frequency responses, corresponding to the first receive and transmit antenna branch $|H_{1,1}|$ of one of the realizations of the tapped delay line

⁵The EVM measurement procedure as described in [24, Annex B for FR1] does not include any wireless channel, but (realistic) impairments stemming from the transmitter such as clipping noise and inband distortion due to nonlinear power amplifier. Therefore, for BS type 1-C and FR1, 3GPP EVM requirements consider linear equalization of the distortion at the receiver, where the distortion is solely emanating from the non-ideal transmitter. In these measurements for 3GPP requirements, the transmitter and receiver are connected with a wire-like connector. Thus, the 3GPP EVM requirements do not consider any wireless channel equalization.

TABLE I: Comparison of computational complexities of various PAPR reduction methods

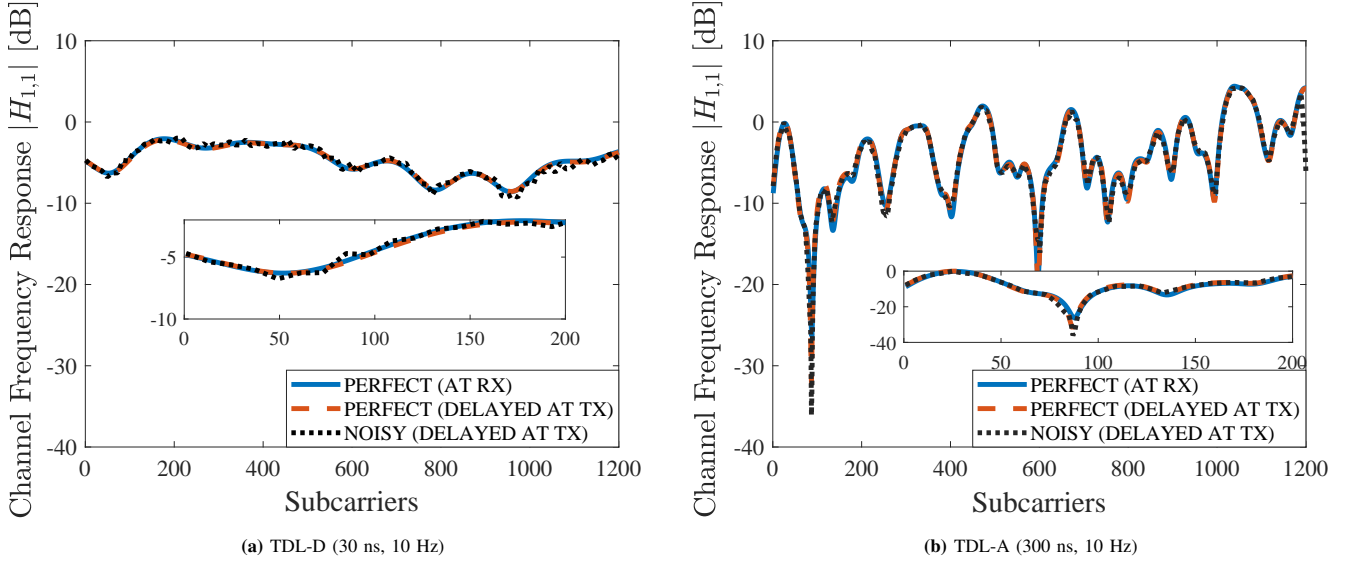
Method	Complexity per (outer) iteration
Prior art (non-CSI-aware): Iterative clip & filter [4]	$\mathcal{O}((N_T \ell K \log(\ell K)))$
Prior art (CSI-aware): Semidefinite relaxation-based [20]	$\mathcal{O}((\ell K N_T)^{4.5})$
Prior art (CSI-aware): Bao et al. [19]	$\mathcal{O}((N_T \ell K (I' + \log(\ell K))) + I_{\max} K_D N_T^2)$; I' and I_{\max} iterations for PROXINF and inner loop, resp.
TOP-ADMM-type: TOP-ADMM/BADMM/DYS	$\mathcal{O}((N_T \ell K \log(\ell K)) + K_D N_T^2)$

TABLE II: Simulation Parameters for 5G NR-like PDSCH

Parameters	Test 1	Test 2
Subcarrier spacing		15 kHz
Carrier bandwidth (PRB allocation)		20 MHz (100 PRBs, <i>i.e.</i> , active subcarriers $N_{SC}=1200$)
DL SU/MU-MIMO N_T, N_R		2/4/8/16/32/64/128/256Tx, 2/4Rx; In MU-MIMO, each user with 1 Rx
Spatial layers (rank)		Fixed rank 2 when $N_R=2$ or 4 when $N_R=4$
Spatial precoding		RZF precoding with regularization $\alpha=0.001$
Precoding resource block group (PRG) size		2 PRBs granularity
Modulation		256QAM
Channel model [50]	TDL-D (30 ns, 10 Hz, K-factor=9)	TDL-A (300 ns, 10 Hz)
MIMO spatial correlation [50]	High-like: $\alpha_1, \alpha_2, \beta=0.9, \gamma=0.3$	Low-like: $\alpha_1, \alpha_2=0.09, \beta=0.03, \gamma=0.0$
DL channel knowledge at the BS		Noisy channel estimate with SNR=5 dB
DL channel knowledge at the UE		Perfect channel estimate
Other information	CSI delay is 1 ms, no additional impairments; fixed $\nu=0.001$ for $\{Q[k]\}$ —cf. (17)	

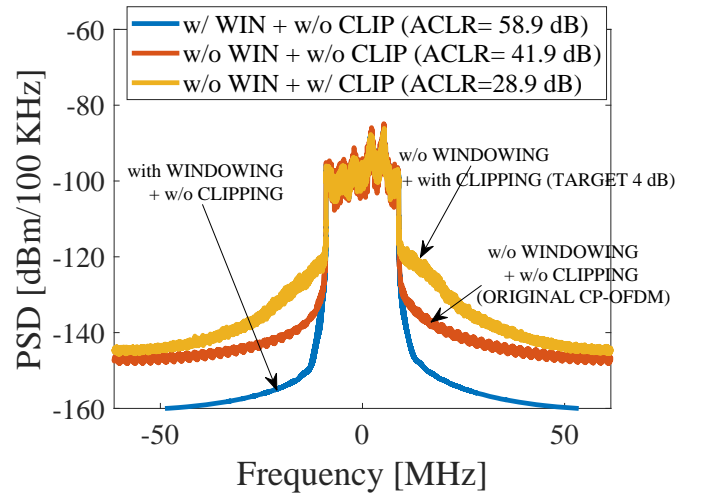
TABLE III: EVM Req. [24]

Modulation Scheme	EVM Threshold
QPSK	17.5%
16QAM	12.5%
64QAM	8.0%
256QAM	3.5%

**Fig. 2:** Magnitude of channel frequency responses $|H_{1,1}|$ of (a) TDL-D (LOS and non-LOS) and (b) TDL-A (non-LOS) channel models.

(TDL) 3GPP NR channel models [49]: TDL-D (30 ns, 10 Hz) in Fig. 2(a) and TDL-A (300 ns, 100 Hz) in Fig. 2(b), where the considered parameters in terms of root mean square delay spread in nano seconds (ns) and maximum Doppler shift in Hz parameters are shown in the brackets. Notice that the taps of the TDL-D channel model follow both Ricean and Rayleigh fading, *i.e.*, line-of-sight (LOS) and non-LOS, whereas the taps of the TDL-A follow only Rayleigh fading, *i.e.*, non-LOS—cf. [49, Section B.2.3.2]. Moreover, we have also extended the 3GPP MIMO channel spatial correlation model for $N_T > 8$ transmit (with cross-polarized antennas) and two/four receive antennas—cf. [50, Section B.2.3.2]. The considered parameters of the MIMO spatial correlation model are given in Table II.

We depict three channel frequency responses in Fig. 2: one at the UE/receiver and two at the base station (BS)/transmitter. At the UE/receiver, perfect channel estimates are utilized for the estimated received EVM. However, at the BS/transmitter, we have employed a channel estimation error model $\mathbf{H} = \hat{\mathbf{H}} + \Delta\mathbf{H}$, where $\Delta\mathbf{H}$ has entries that are independent and identically distributed and follow zero mean circularly sym-

**Fig. 3:** PSD of OFDM waveform with and without (raised cosine) transmit windowing.

metric complex Gaussian distribution with given variance $\tilde{\sigma}_{ce}^2$. The noisy channel estimates $\hat{\mathbf{H}}$ with $\text{SNR} = -10 \log_{10}(\tilde{\sigma}_{ce}^2) = 5$ dB are used both for MIMO signal precoding and computa-

tion of \mathbf{Q} matrices as defined in (17). Both MIMO signal precoding \mathbf{W} and \mathbf{Q} matrices have two physical resource blocks (PRBs) for grouping—see Table II—which implies that the mean channel estimate within considered precoding resource block group (PRG) is used for the computation of \mathbf{W} and \mathbf{Q} .

In Fig. 3, we illustrate three plots of power spectral density (PSD) of the OFDM waveform having a useful signal bandwidth of 20 MHz, see Table II, 1) without either transmit windowing or any PAPR reduction method, 2) with transmit windowing but without any PAPR reduction method, and 3) with a naïve amplitude clipping (PAPR target of 4 dB) but without any transmit windowing. The transmit windowing is typically employed to shape the spectrum to meet the minimum 3GPP NR ACLR requirement of 45 dB [24], see, *e.g.*, [35], [38], [51]. In this study, we perform transmit windowing—using raised cosine windowing, see, *e.g.*, [51]—after the (proposed) PAPR reduction if enabled. Although windowing penalizes $\sim 10\%$ of the cyclic prefix, the spectrum-shaped signal has 58.9 dB of ACLR, which clearly meets the minimum 45 dB ACLR requirement (with a good implementation margin). However, as we show in the PSD result subsequently, depending on the ACLR constraint ψ_{aclr} , the effective ACLR after the (proposed) PAPR reduction method(s) can be lower than ~ 59 dB but must be more than or equal to 45 dB (with some margin) to comply with the requirement. Clearly, distortion-based PAPR reduction methods, such as clipping, require filtering or windowing to remove unwanted distortion on the unused subcarriers.

B. Simulation Results

In this section, we present the simulation results for the test cases given in Table II. We consider TOP-ADMM-type performance with iteration-dependent sets targeting problem P3 unless specified explicitly. Additionally, we set $\zeta=0$ typically for the computation of the gradient of h in (21) unless stated otherwise. Moreover, the typical MIMO test setup is 64 transmit antennas, and two receive antennas unless mentioned otherwise. Since the estimated EVM at the receiver is computed for each spatial layer—see Section III-B2—we do not differentiate between SU-MIMO and MU-MIMO performance evaluation.

We have employed linear regularized zero forcing (RZF)-based MIMO (spatial) precoding in the downlink, which can be expressed as $\mathbf{X}[:, k] = \mathcal{W}(\mathbf{S}[:, k]) = \mathbf{W}[k]\mathbf{S}[:, k]$, where the MIMO precoder reads $\mathbf{W}[k] = \Xi \odot \widetilde{\mathbf{W}}[k]$, where Ξ normalizes power discussed later in the following text. The un-normalized RZF as given by, see, *e.g.*, [52], is $\mathbb{C}^{N_T \times N_L} \ni \widetilde{\mathbf{W}}[k] = \widehat{\mathbf{H}}[k]^H (\widehat{\mathbf{H}}[k] \widehat{\mathbf{H}}[k]^H + \widetilde{\mathbf{R}} + \alpha \mathbf{I}_{N_R})^{-1} := [\widetilde{\mathbf{w}}_1[k], \dots, \widetilde{\mathbf{w}}_{N_L}[k]]$. The choice of suitable regularizing parameters, namely Hermitian positive semidefinite $\widetilde{\mathbf{R}}$ and $\alpha \in \mathbb{R}_{\geq 0}$, are typically tunable to maximize the desired performance metrics of the system, such as the sum-rate, see, *e.g.*, [52]. Moreover, the power normalization matrix can be $\mathbb{C}^{N_T \times N_L} \ni \Xi = \left[\frac{\sqrt{\eta_1}}{\|\widetilde{\mathbf{w}}_1[k]\|_2} \mathbf{1}_{N_T}, \dots, \frac{\sqrt{\eta_{N_L}}}{\|\widetilde{\mathbf{w}}_{N_L}[k]\|_2} \mathbf{1}_{N_T} \right]$, where $\{\sqrt{\eta_s}\}$ is a set of powers that can be assigned to respective layers or users. Consequently, the total power allocated to the k -th subcarrier

must satisfy $\|\mathbf{W}[k]\|_F^2 = \sum_{s=1}^{N_L} \eta_s$. In our simulations, we have simply set Ξ as all-ones matrix.

Most of all, to motivate the signal distortion-based PAPR reduction schemes for 5G NR and beyond, in Fig. 4, we compare the distortion-based PAPR reduction techniques, notably, classical iterative clipping and frequency-domain filtering (ICF) [4] and our proposed TOP-ADMM with two variants of signal distortion-less tone reservation (TR) schemes under a special case with a single transmit and receive antenna. In ICF, let $\mathbb{C}^{K \times N_T} \ni \mathbf{T} = \mathbf{F}^H \mathbf{X}^T$ be a time-domain input signal; $\overline{\mathbf{T}}^{(I)}$ denotes a time-domain output from ICF after I iterations. Then, within one iteration cycle of ICF, for each j -th transmit antenna and an i -th iteration, the amplitude of a discrete time-domain (oversampled) signal is clipped $\overline{\mathbf{T}}^{(i)}[n, j] = A \exp\{\iota \phi(n)\}$ if $|\overline{\mathbf{T}}^{(i-1)}[n, j]| > A$, where $A = \sqrt{\gamma_{\text{par}} P_{\text{avg}}}$, P_{avg} is average transmit power of the signal, and $\phi(n)$ is the phase of $\overline{\mathbf{T}}^{(i-1)}[n, j]$. In the frequency-domain of a clipped signal, the unwanted distortions on the unused/inactive subcarriers are zeroed out. After filtering, the frequency-domain signal is transformed back to the time-domain signal. We repeat this time-domain and frequency-domain filtering for I iterations. For tone reservation schemes, there are at least two popular variants: 1) unconstrained method, referred to as TR1, *i.e.*, minimize $\|\mathbf{F}^H (\mathbf{X} + \overline{\mathbf{C}})\|_\infty$, where $\overline{\mathbf{C}}$ corresponds to tones/subcarriers in the guard bands, and 2) peak-constrained method, called TR2, *i.e.*, $\|\overline{\mathbf{C}}\|_F \leq \text{threshold}$. In the unconstrained TR1 scheme, the energy of the subcarriers carrying PAPR reduction capable information does not have any constraint/restriction on the energy. Therefore, the unconstrained TR1 method causes peaks, see Fig. 4(a) for 24 tones (CCs) on each edge of guard bands, on the power spectral density, which can cause many radio frequency-related implementation issues, including PA linearization. Hence, the peak-constrained TR2 technique can control the peaks but penalizes the capability to reduce the PAPR of signal—see Fig. 4(b) constraining the total energy of 36 CCs for TR2 within 5% of total energy for useful signal. Additionally, we cannot use many unused tones due to the strict compliance with the regulatory and 3GPP standard spectral mask requirements. For high numerical accuracy of solutions of TR1 and TR2 schemes, we employ CVX since TR1/TR2 does not offer closed-form solutions due to the minimization of the infinite norm. Noticeably, although TR1 and TR2 schemes offer relatively low complexity compared to our proposed TOP-ADMM method, TR1 and TR2, unfortunately, cannot meet desired PAPR targets under practical constraints—see Fig. 4(b). Moreover, recall that the guard bands of NR/LTE can be used to deploy NB-IoT carriers, among other practical challenges for the PAPR reduction in NR/LTE.

Figure 5 illustrates the complementary cumulative distribution function (CCDF) of IPAPR considering cell-specific broadcast/control channel or non-CSI-aware, *i.e.*, the base station has no downlink channel knowledge, under Test 2 (see Table II) but with a single antenna at the transmitter and the receiver. By the formulation of our proposed problem P3/P4, it can fall back and support the case where the base station

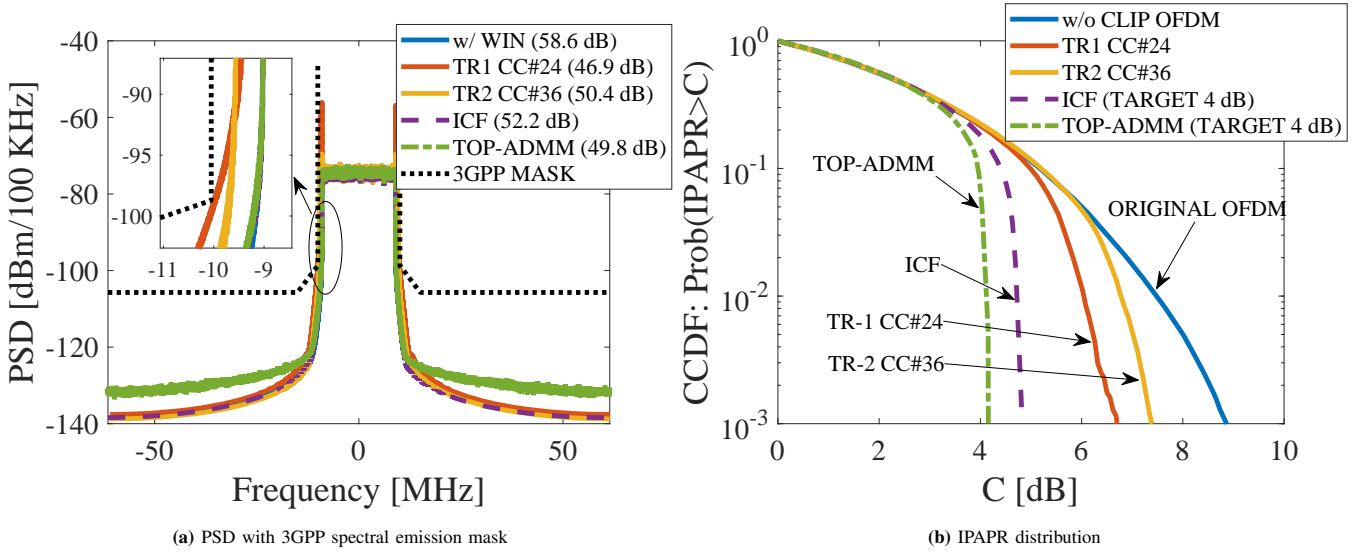


Fig. 4: Comparison among 1) distortion-based: ICF and (non-CSI-aware) TOP-ADMM, and 2) distortion-less: TR1 and TR2. Noticeably, TR1/TR2 has poor PAPR reduction performance compared to ICF/TOP-ADMM.

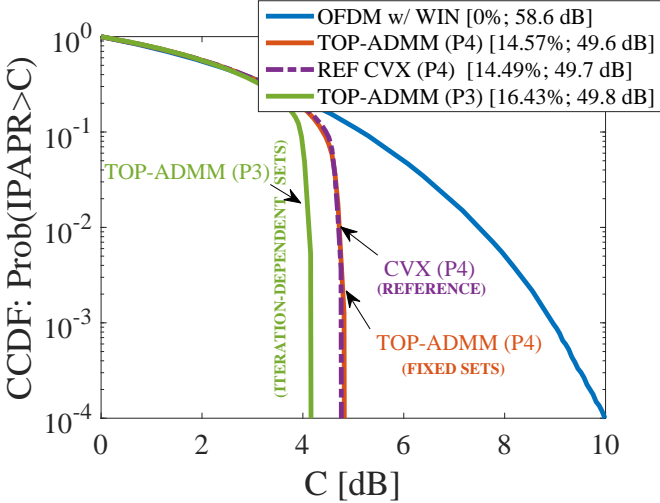


Fig. 5: Broadcast channel: IPAPR distribution comparison between P3 (with iteration-dependent sets) and P4 (with fixed sets).

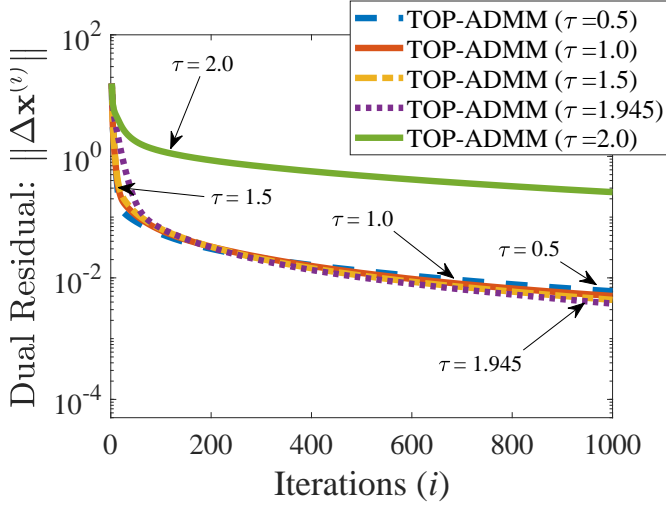
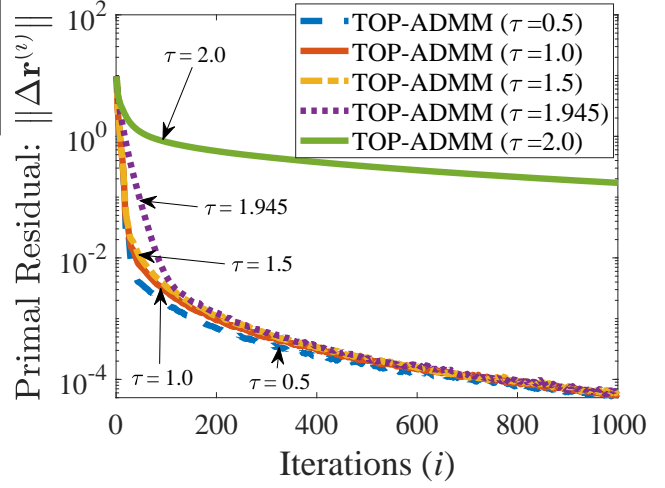
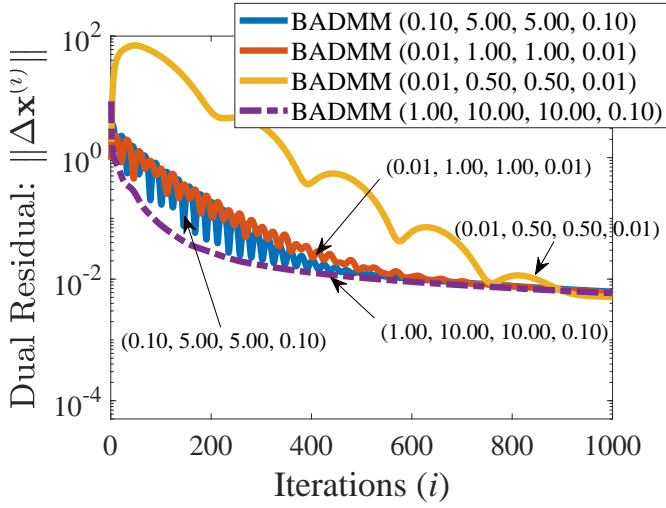
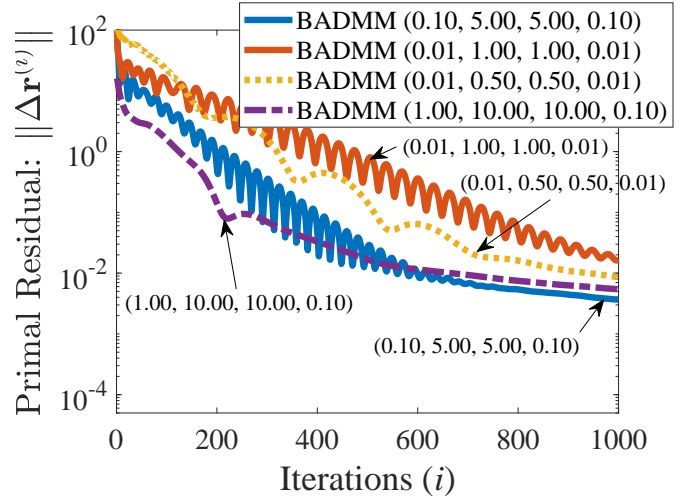
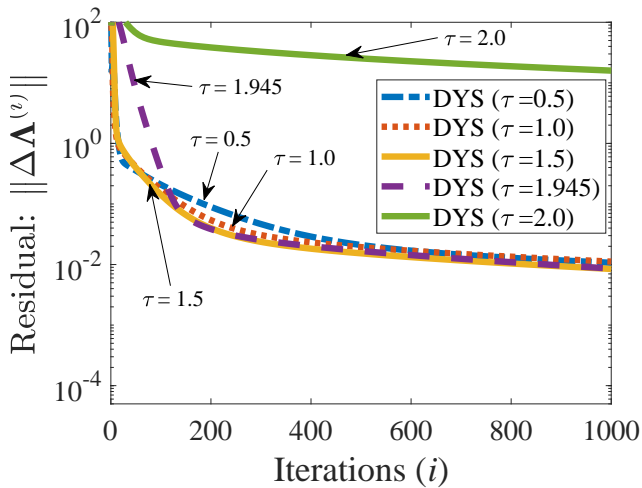
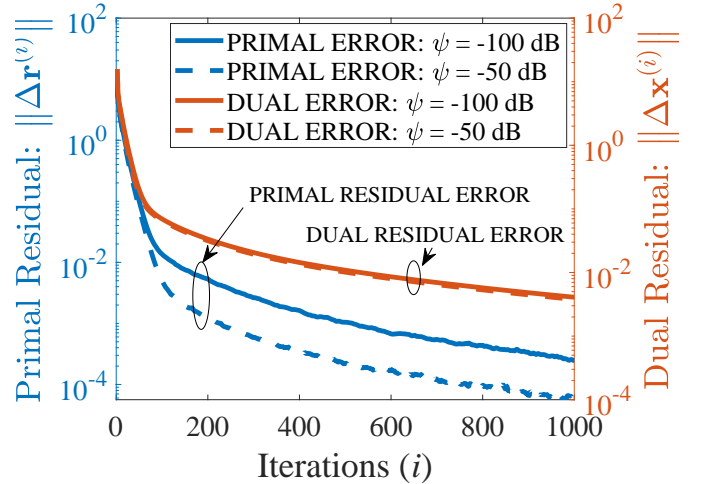
has no downlink channel knowledge, which can cover the cell-specific broadcast/control channel case, *e.g.*, by setting $\{Q[k] = \nu I\}$ with $\nu \geq 0$ —see (17)—and $\zeta \geq 0$. For brevity, we have set the following parameters to evaluate P3/P4 for the non-CSI-aware case: $\nu = 0$, *i.e.*, $Q[k] = 0$ and $\zeta = 0.05$. For TOP-ADMM, we have set the step-size $\tau = 1.945$ targeting either P3 or P4. As expected by our conjecture, TOP-ADMM targeting P3, *i.e.*, with iteration-dependent sets, yields a better solution—at least not worse—than TOP-ADMM targeting P4 in terms of PAPR. Moreover, our proposed computationally efficient TOP-ADMM-based solution targeting P4 converges to a similar solution using, high numerical accuracy, CVX wrapper (with SDPT3 solver) [47]. However, CVX is very slow to run on a personal computer even for single antennas. Therefore, we could not obtain solutions using CVX for P4 with more than one antenna. Under the non-CSI-aware case, the proposed problem P3 or P4 minimizes the transmit EVM subject to the PAPR and ACLR constraints. In the sequel,

we show numerically that when the base station with many antennas has (practically even imperfect) downlink channel estimates, the proposed problem P3 or P4—solved by using our implementation-friendly TOP-ADMM-based algorithms—mitigates the signal distortion seen at the receiver by capitalizing on the excess spatial degrees of freedom.

For benchmarking purposes, we evaluate ICF [4] as a baseline for distortion-based PAPR reduction techniques. Additionally, we evaluate the prior art, in particular the method referred to as PROXINF-ADMM1, which essentially targets to solve convex programming problem [19, Equation (14)/(15)]. Observe that the authors in [19] employed double loops, which can be avoided by directly employing our (proposed) three-operator ADMM-like approaches.

Figures 6–8 exhibit the convergence behaviour of the (proposed) TOP-ADMM-type algorithms, namely, TOP-ADMM (Algorithm 1), BADMM (Algorithm 2), and DYS (Algorithm 3). We use a set of tunable parameters to solve the optimization problem P3 considering Test 1 with four transmit and two receive antennas—see Table II—for PAPR constraint with $\gamma_{\text{par}} = 4$ dB and ACLR constraint with $\psi_{\text{aclr}} = -50$ dB. We do not know an optimal solution to problem P3 a priori (or through any black-box global optimization solvers). Thus, as remarked in [26], we characterize the convergence of the (proposed) TOP-ADMM-type algorithms, see Figure 6, and BADMM, see Figure 7, in terms of the primal and dual residual errors, *i.e.*, $\|\Delta \mathbf{r}^{(i)}\| := \|\bar{\mathbf{Y}}^{(i)} - \bar{\mathbf{X}}^{(i)}\|_F$ and $\|\Delta \mathbf{x}^{(i)}\| := \|\bar{\mathbf{X}}^{(i)} - \bar{\mathbf{X}}^{(i-1)}\|_F$, respectively. For the convergence analysis of DYS (Algorithm 3), the (fixed-point) residual error, *cf.* [32], $\|\Delta \Lambda^{(i)}\| := \|\Lambda^{(i)} - \Lambda^{(i-1)}\|_F$ plays a similar role as the primal and dual residual errors—see Figure 8.

In TOP-ADMM (Algorithm 1), the scaled dual variable $\Lambda^{(i+1)}/\rho$ could be used such that Algorithm 1 becomes free from the ρ parameter. Consequently, Algorithm 1 has only one tunable step-size τ parameter. In Fig. 6, we show the residual errors for the step-size $\tau \in \{0.500, 1.000, 1.500, 1.945, 2.000\}$.

(a) TOP-ADMM (τ): Dual residual vs. Iterations(b) TOP-ADMM (τ): Primal residual vs. Iterations**Fig. 6:** Algorithm 1 convergence behaviour(a) BADMM ($\rho, \rho_x, \rho_z, \tau$): Dual residual vs. Iterations(b) BADMM ($\rho, \rho_x, \rho_z, \tau$): Primal residual vs. Iterations**Fig. 7:** Algorithm 2 convergence behaviour.**Fig. 8:** DYS (τ), Algorithm 3, convergence behaviour**Fig. 9:** Convergence behaviour of TOP-ADMM($\tau = 1.945$) with $\psi_{\text{acrlr}} \in \{-50, -100\}$ dB

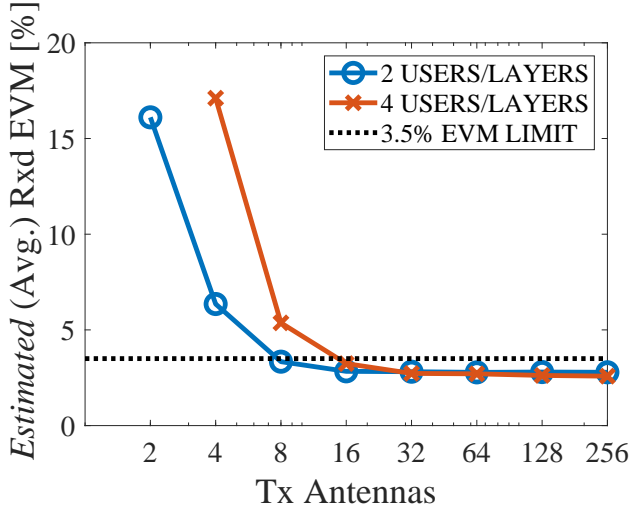


Fig. 10: Estimated average received EVM against increasing excess spatial degrees of freedom for $N_T \times 2$ and $N_T \times 4$ DL MU-MIMO/SU-MIMO setup under Test 2.

Similar to TOP-ADMM with a scaled dual variable, the DYS-based Algorithm 3 also has only one parameter, where Fig. 8 illustrates the primal and dual residual errors against iterations for various step-sizes $\tau \in \{0.500, 1.000, 1.500, 1.945, 2.000\}$. In contrast to TOP-ADMM and DYS, the BADMM algorithm is not blessed with a single parameter but with four parameters $(\rho, \rho_x, \rho_z, \tau)$. In Fig. 7, the primal and dual residual errors are shown for some choices of parameters within a bracket. Conspicuously, the primal residual error of the sequences generated by TOP-ADMM is nearly 10 times smaller than the BADMM. Although these metrics, *i.e.*, primal and residual errors, are commonly used in the (numerical) optimization literature, subsequently, we focus directly on the performance metrics of interest against iteration. Nevertheless, from these numerical convergence figures, we fix the tunable parameters of the respective algorithms for the subsequent performance figures. Therefore, for TOP-ADMM, BADMM, and DYS, we use $\tau = 1.945$, $(\rho = 0.01, \rho_x = 1, \rho_z = 1, \tau = 0.01)$, and $\tau = 1.945$, respectively, unless mentioned otherwise. Additionally, in Fig. 9, we show the convergence behaviour of TOP-ADMM for two different ACLR constraints having $\psi_{\text{aclr}} \in \{-50, -100\}$ dB. In terms of primal residual error, the convergence noticeably improves with the relaxed ACLR constraint having $\psi_{\text{aclr}} = -50$ dB. Similar behaviour is observed with BADMM and DYS. To this end, we fix both ACLR and PAPR constraints with $\psi_{\text{aclr}} = -50$ dB and $\gamma_{\text{par}} = 4$ dB, respectively, unless stated otherwise.

Figure 10 shows the inband performance with increasing excess spatial degrees of freedom, *i.e.*, number of transmit antennas under Test 2 using TOP-ADMM (targeting P3) with the above discussed fixed parameters. More specifically, this figure depicts the estimated (averaged) received EVM performance of MU-MIMO or SU-MIMO with 2/4 users or spatial layers against increasing excess spatial degrees of freedom. As expected, the proposed problem P3 (or P4) mitigates the incurred signal distortion when there are good enough excess spatial degrees of freedom. However, the estimated

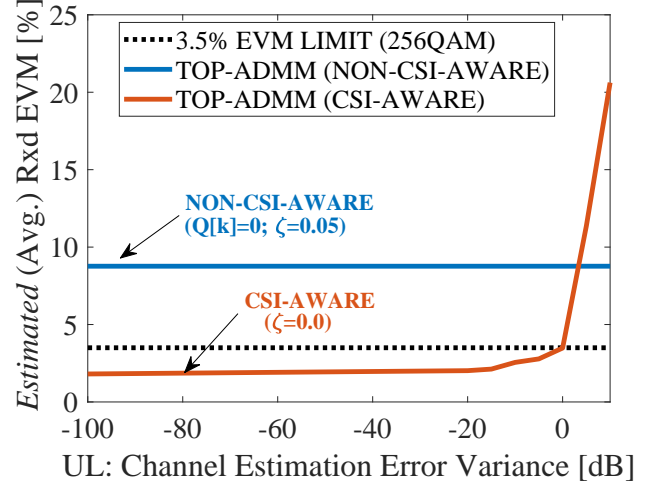


Fig. 11: Estimated average received EVM against increasing UL channel estimation error variance with a fixed regularizer $\nu = 0.001$ for $\{Q[k]\}$ —cf. (17)—under Test 2.

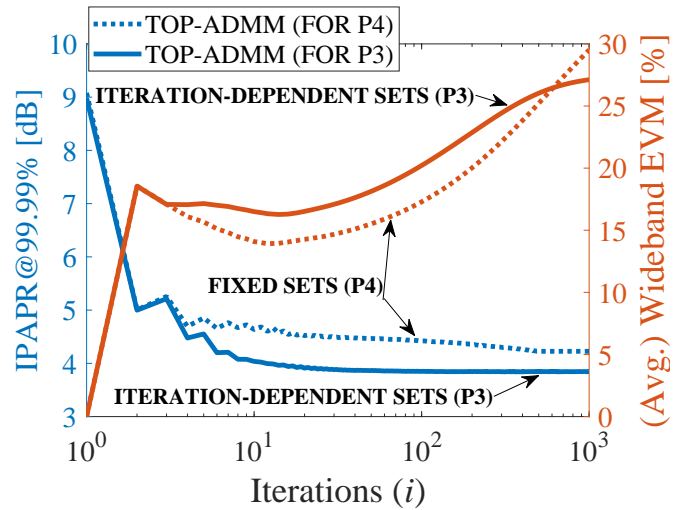


Fig. 12: CSI-aware: Comparison between TOP-ADMM (for P3 with iteration-dependent sets) and TOP-ADMM (for P4 with fixed sets) under Test 1.

received EVM may not necessarily vanish entirely or become zero with very high excess spatial degrees of freedom due to many practical reasons such as imperfect channel estimates and channel aging.

Figure 11 illustrates the robustness against the usage of erroneous channel estimates with a fixed regularizer $\nu = 0.001$ in the computation of distortion mitigation $\{Q[k]\}$ —see. (17)—under Test 2. The channel estimation error variance equal to -100 dB represents perfect channel estimates at the transmitter. Therefore, as expected, the received EVM increases if the channel estimation error variance increases. Hence, if channel estimation error variance is high, then one can instead make the proposed PAPR reduction without capitalizing on the CSI knowledge if any, *e.g.*, by simply setting $\{Q[k] = 0\}$ and $\zeta = 0.05$, *i.e.*, the fall back mode, where P3/P4 minimizes the transmit EVM as required for the broadcast/control channel (or non-CSI-aware case). Additionally, the practical system employs a link adaptation, where the modulation and coding

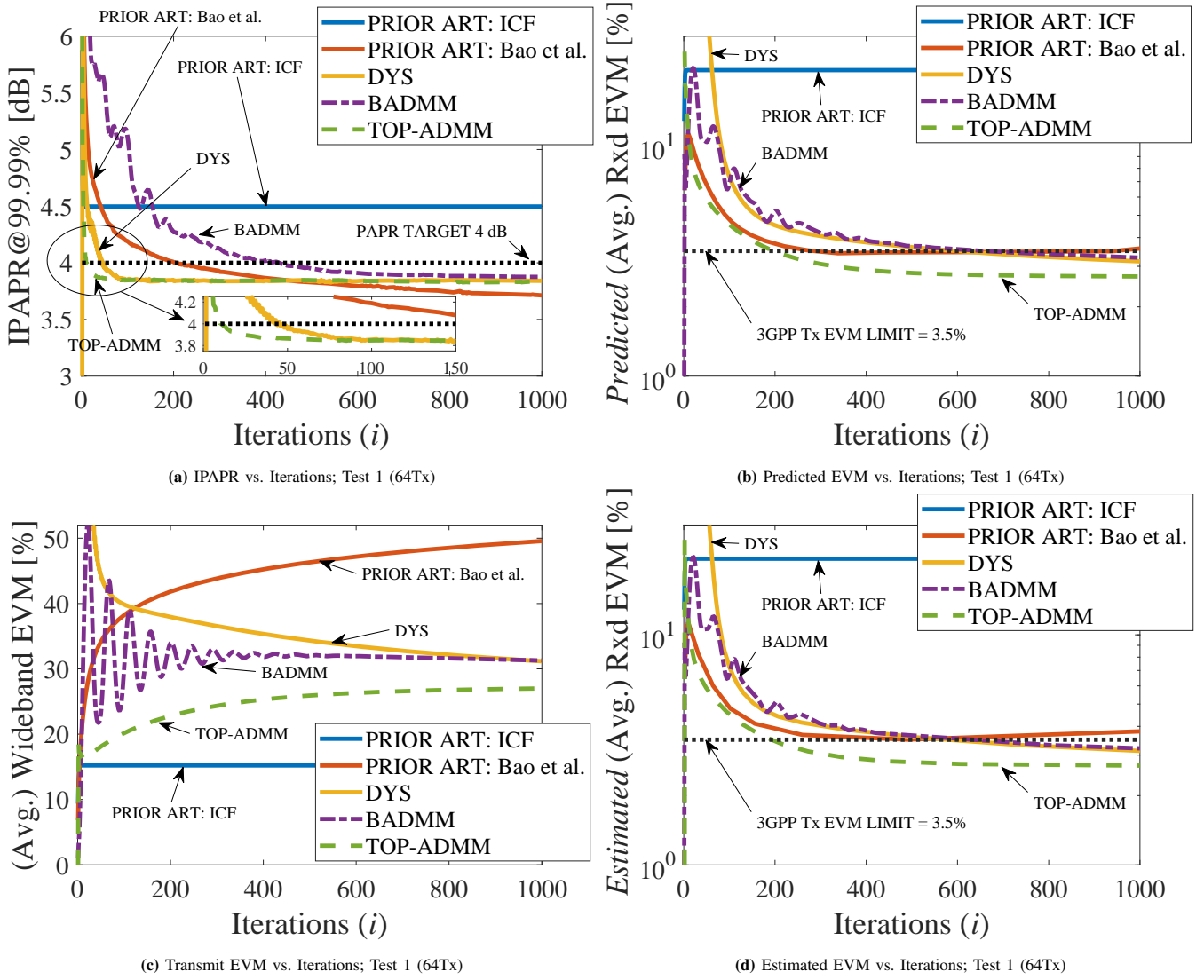


Fig. 13: Performance comparison of proposed TOP-ADMM-type algorithms (at PAPR target of 4 dB) with two prior arts, namely the non-CSI-aware ICF [4] and CSI-aware Bao et al. algorithm [19] in Test 1.

scheme for the downlink transmission can be adapted according to the channel conditions (via CSI report feedback). In Fig. 12, we compare the TOP-ADMM solution achieved by solving P_3 with P_4 considering Test 1 (64×2 MIMO setup). As expected, the solution of P_3 (utilizing iteration-dependent sets) renders better performance than the solution of P_4 (using fixed constraint sets).

Figure 13 compares the performance metrics against iterations of proposed TOP-ADMM-type methods with the two considered prior arts. Note that the prior art by Bao et al. [19] has two inner iterations for each outer iteration, which are included in these plots for a fair comparison. Figure 13(a) shows the achieved IPAPR at 99.99% probability within each OFDM symbol. Clearly, TOP-ADMM followed by DYS has a relatively faster convergence compared to BADMM. One of the reasons for the slower convergence of BADMM among the proposed methods could be due to the curse of the number of tuning parameters. In other words, a better and finer grid search of tunable parameters of BADMM may be required to be competitive. Nevertheless, we iterate that the target

optimization problem in [19] minimizes signal peaks subject to equality constraints on EVM mitigation and ACLR. However, in practice, we need to adjust at least one of the performance metrics, *i.e.*, PAPR or EVM, according to the traffic and channel conditions. Therefore, the method in [19] achieves the ~ 0.25 dB smaller IPAPR than the proposed methods but at the cost of a nearly two-fold increase in transmit EVM, see Fig. 13(c). This two times increase in the transmit EVM, *i.e.*, ~ 6 dB increase in the distortion energy, consequently penalizes the energy of the useful transmit signal by ~ 6 dB since the total transmit power is fixed and shared by both the signal and distortion. It can clearly be argued that this IPAPR gain is worthwhile in practice. Moreover, for a larger modulation alphabet, such as 1024QAM in the upcoming NR releases, a lower estimated received EVM would be required compared to 256QAM. Thus, one might need to lower the target PAPR (or back off). Hence, the optimization problem (and method) proposed in [19] would be unfortunately and arguably impractical for realistic radio systems. Furthermore, Figs. 13(b),(d) illustrate the predicted and estimated EVM,

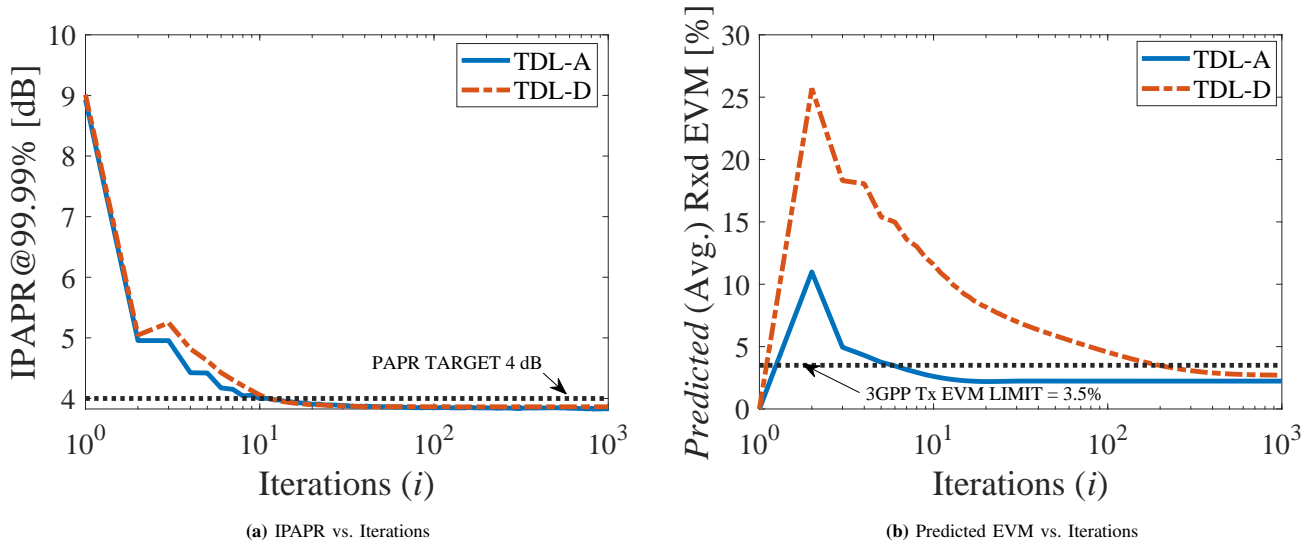


Fig. 14: TOP-ADMM: Test 2 (TDL-A; Non-LOS, low spatial corr.) vs. Test 1 (TDL-D; LOS+Non-LOS, high spatial corr.).

respectively, over iterations. All the methods except ICF meet the desired estimated EVM target of 5.6% (additionally, as a reference, we have also shown the 3GPP transmit EVM requirement of 3.5% for 256QAM). However, TOP-ADMM has slightly better estimated/predicted received EVM performance compared to DYS and BADMM, and noticeably compared to prior arts.

In Fig. 14, we compare TOP-ADMM performance in terms of IPAPR and predicted received EVM against the iterations achieved in Test 1, *i.e.*, the TDL-D channel model with non-LOS and LOS components and high-like spatial correlation, and in Test 2, *i.e.*, the TDL-A channel model with only non-LOS components and low-like spatial correlation. We construe the following key observation from this plot.

Observation 1. *The convergence, in terms of the predicted/estimated received EVM over iterations, slows down for a channel with increasing Rician K -factor, *i.e.*, LOS component, and spatial correlation.*

The slower convergence under such channel conditions could be due to more active constraints.

For completeness, Fig. 15 presents the scatter plot, PSD, and EVM distribution after the last considered iteration (simply fixed to 1000 for all the algorithms) of ICF, the Bao et al. method, and TOP-ADMM. Note that we average the EVM and PSD metrics over 28 OFDM symbols to analyze instantaneous-like behaviour. In Figs. 15(a)–(c), we illustrate the scatter plot of estimated/equalized received symbols for ICF, the Bao et al. method, and TOP-ADMM, respectively. Incontestably, the scatter plot of TOP-ADMM shows qualitatively the lowest estimated received EVM compared to prior arts (particularly, the CSI-aware Bao et al. method). We show the distribution of the average (over time domain OFDM symbols) estimated received EVM for Spatial Layers 1 and 2 across subcarriers in Fig. 15(d),(e), respectively. Clearly, for the non-robust Bao et al. method, in some sets of subcarriers, we observe high amounts of estimated received EVM compared to not only TOP-ADMM but also classical ICF. The estimated received

EVM in some resources can be large due to the composite mismatch effect under channel uncertainty. In Fig. 15(f), we also depict the (normalized) throughput against the average SNR per receive antenna after the respective PAPR reduction algorithms with link adaptation enabled under Test 1. Around 20 dB SNR, we see that prior art [19] performs poorer than our method. The reason is that the method in [19] renders high transmit signal distortion energy, see Fig. 13(c), which consequently penalizes the useful signal’s transmit energy. However, as expected, at high enough SNR, our proposed TOP-ADMM and the method in [19] will have a negligible impact on the throughput performance.

VI. CONCLUSION

In this paper, we sought a principled approach to mitigate (CSI-aware catering to user-specific beamformed channel under channel uncertainty) or minimize (non-CSI-aware supporting cell-specific non-beamformed broadcast channel) flexibly signal distortion seen at the receivers subject to nonconvex PAPR and ACLR constraints for a large-scale MIMO-OFDM-based system. Unfortunately, a general-purpose solver for such a large-scale (nonconvex) optimization problem is practically infeasible. Hence, to tackle such a nonconvex problem, we applied iteration-dependent “convexification” to the nonconvex PAPR and ACLR constraints. We conjecture that such iteration-dependent “convexification” approaches the nonconvex constraint set asymptotically. Furthermore, we capitalized on a divide-and-conquer approach to decompose the large-scale problem into smaller easy-to-solve subproblems. More concretely, we proposed a powerful and simple optimization solution using our recently proposed TOP-ADMM algorithm to tackle such a problem and compared it to two relatively new algorithms popular within machine learning and (numerical) optimization, the so-called BADMM and DYS algorithms. Consequently, we developed three “implementation-friendly” algorithms to tackle the proposed large-scale (nonconvex) optimization problem. Numerical results showed that the proposed low-complexity algorithms can meet the estimated (received)

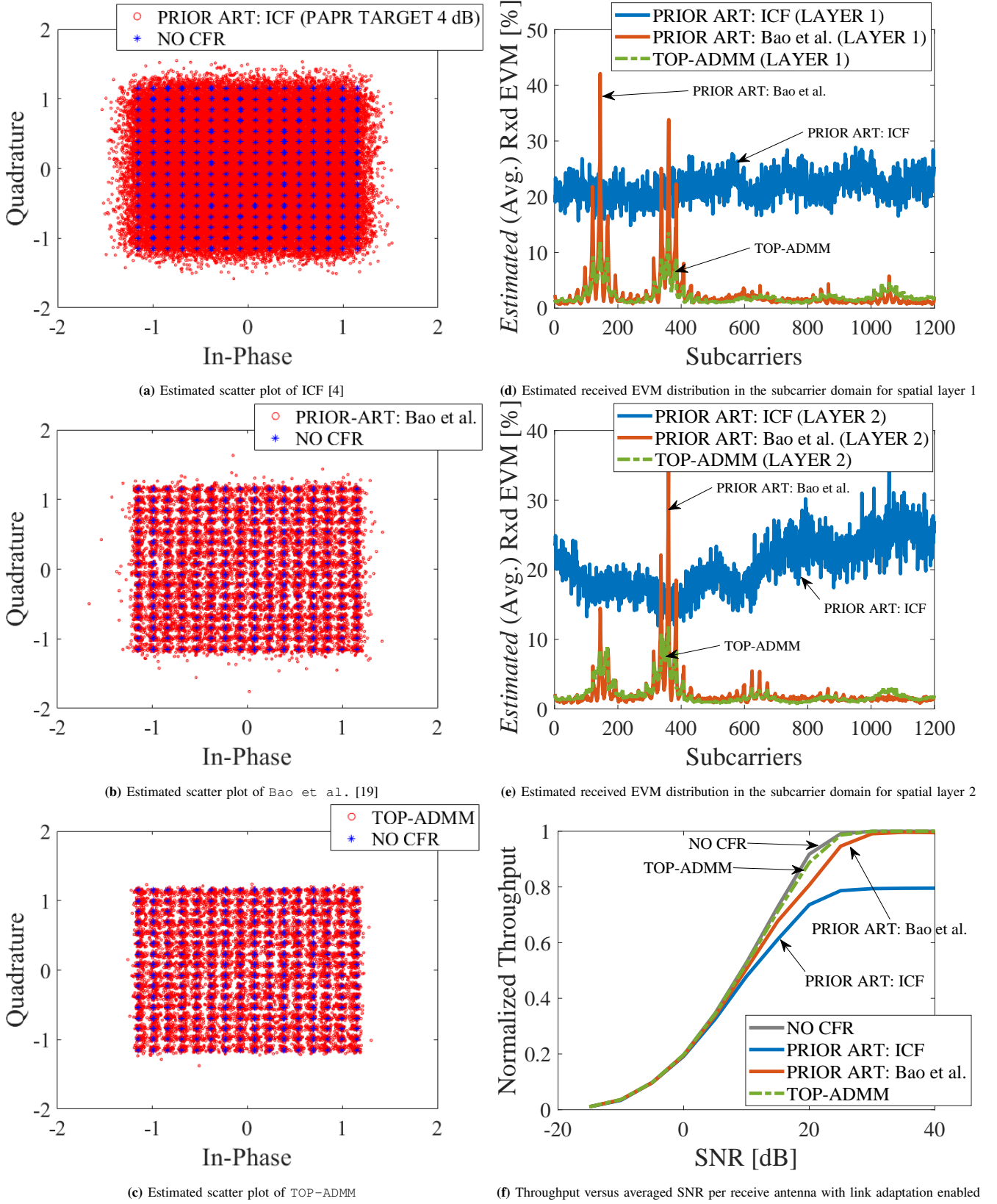


Fig. 15: Scatter plot, EVM, ACLR, and Throughput performance comparison of TOP-ADMM with prior art.

EVM target while meeting the desired PAPR and ACLR constraints. This is arguably the first work to propose computationally efficient algorithms for a robust EVM mitigation problem under channel uncertainty with nonconvex PAPR and

ACLR constraints.

APPENDIX A

OPTIMALITY CONDITIONS OF TOP-ADMM FOR P3/P4

We first form the Lagrangian to (19) (considering in (7) form)—no convexity assumptions are required:

$$\mathcal{L}(\bar{\mathbf{X}}, \bar{\mathbf{Z}}, \Lambda) := \delta_{\mathcal{U}}(\bar{\mathbf{X}}) + \delta_{\mathcal{P}}(\bar{\mathbf{Z}}) + h(\bar{\mathbf{Z}}) + 2\Re\{\text{Tr}[\Lambda^H(\bar{\mathbf{X}} - \bar{\mathbf{Z}})]\}.$$

It is known that the KKT conditions are first-order optimality conditions which are necessary conditions for the solution point of (7) to be optimal under some suitable constraint qualifications, see, *e.g.*, [23]. Then, we assume the sub-differential exist for the (nonconvex) indicator function. Let $[\bar{\mathbf{X}}^*; \bar{\mathbf{Z}}^*; \Lambda^*]$ be a KKT point, which fulfils the dual feasibility, *i.e.*, $\mathbf{0} \in \partial \delta_{\mathcal{U}}(\bar{\mathbf{X}}^*) + \Lambda^*$ and $\mathbf{0} \in \partial \delta_{\mathcal{P}}(\bar{\mathbf{Z}}^*) + \nabla h(\bar{\mathbf{Z}}^*) - \Lambda^*$ and the primal feasibility, *i.e.*, $\bar{\mathbf{X}}^* - \bar{\mathbf{Z}}^* = \mathbf{0}$. Following [35, Appendix B], we can easily show that the sequences generated by TOP-ADMM for either P3 (under the conjecture that the residual errors vanish asymptotically) or P4 (see [46]), at any limit point, converges to a KKT point.

REFERENCES

- [1] S. Kant, M. Bengtsson, B. Göransson, G. Fodor, and C. Fischione, “Robust PAPR reduction in large-scale MIMO-OFDM using three-operator ADMM-type techniques,” in *2021 55th Asilomar Conference on Signals, Systems, and Computers*, 2021, pp. 616–622.
- [2] E. Dahlman, S. Parkvall, and J. Sköld, *5G NR: The next generation wireless access technology*. Academic Press, 2018.
- [3] R. Prasad, *OFDM for wireless communications systems*. Artech House, 2004.
- [4] J. Armstrong, “Peak-to-average power reduction for OFDM by repeated clipping and frequency domain filtering,” *Electron. Lett.*, vol. 38, no. 5, pp. 246–247, Feb. 2002.
- [5] Y.-C. Wang and Z.-Q. Luo, “Optimized iterative clipping and filtering for PAPR reduction of OFDM signals,” *IEEE Trans. Commun.*, vol. 59, no. 1, pp. 33–37, Jan. 2011.
- [6] P. Börjesson, H. G. Feichtinger, N. Grip, M. Isaksson, N. Kaiblinger, P. Ödling, and L. Persson, “A low-complexity PAR-reduction method for DMT-VDSL,” in *Proc. 5th International Symposium on Digital Signal Processing for Communications Systems (DSPCS)*, Perth, Australia, Feb. 1999, pp. 164–169.
- [7] T. Kageyama, O. Muta, and H. Gacanin, “Performance analysis of OFDM With peak cancellation under EVM and ACLR restrictions,” *IEEE Trans. Veh. Technol.*, vol. 69, no. 6, pp. 6230–6241, Jun. 2020.
- [8] X. Wang, T. Tjhung, and C. Ng, “Reduction of peak-to-average power ratio of OFDM system using a companding technique,” *IEEE Trans. Broadcast.*, vol. 45, no. 3, pp. 303–307, Sep. 1999.
- [9] J. Davis and J. Jedwab, “Peak-to-mean power control in OFDM, Golay complementary sequences, and Reed-Muller codes,” *IEEE Trans. Inf. Theory*, vol. 45, no. 7, pp. 2397–2417, Nov. 1999.
- [10] R. W. Bäuml, R. F. H. Fisher, and J. B. Huber, “Reducing the peak-to-average power ratio of multicarrier modulation by selected mapping,” *IEEE Electronic Letters*, vol. 32, no. 22, pp. 2056–2057, Oct. 1996.
- [11] J. Tellado and J. M. Cioffi, “Peak power reduction for multicarrier transmission,” in *Proc. IEEE Global Communications Conference (GLOBECOM)*, Sydney, Australia, Nov. 1998.
- [12] Seung Hee Han and Jae Hong Lee, “An overview of peak-to-average power ratio reduction techniques for multicarrier transmission,” *IEEE Wireless Commun.*, vol. 12, no. 2, pp. 56–65, Apr. 2005.
- [13] Y. Rahmatallah and S. Mohan, “Peak-to-average power ratio reduction in OFDM systems: A survey and taxonomy,” *IEEE Commun. Surveys Tuts.*, vol. 15, no. 4, pp. 1567–1592, 4th Quart., 2013.
- [14] G. Wunder, R. F. H. Fischer, H. Boche, S. Litsyn, and J. No, “The PAPR problem in OFDM transmission: New directions for a long-lasting problem,” *IEEE Signal Process. Mag.*, vol. 30, no. 6, pp. 130–144, Nov. 2013.
- [15] D. Mestdagh and P. Spruyt, “A method to reduce the probability of clipping in DMT-based transceivers,” *IEEE Trans. Commun.*, vol. 44, no. 10, pp. 1234–1238, 1996.
- [16] Y. Wang, S. Xie, and Z. Xie, “FISTA-based PAPR reduction method for tone reservation’s OFDM system,” *IEEE Wireless Commun. Lett.*, vol. 7, no. 3, pp. 300–303, 2018.
- [17] B. Krongold and D. Jones, “PAR reduction in OFDM via active constellation extension,” *IEEE Trans. Broadcast.*, vol. 49, no. 3, pp. 258–268, 2003.
- [18] C. Studer and E. G. Larsson, “PAR-aware large-scale multi-user MIMO-OFDM downlink,” *IEEE Journal on Selected Areas in Communications*, vol. 31, no. 2, pp. 303–313, Feb. 2013.
- [19] H. Bao, J. Fang, Q. Wan, Z. Chen, and T. Jiang, “An ADMM approach for PAPR reduction for large-scale MIMO-OFDM systems,” *IEEE Trans. Veh. Technol.*, vol. 67, no. 8, pp. 7407–7418, Aug. 2018.
- [20] M. Yao, M. Carrick, M. M. Sohel, V. Marojevic, C. D. Patterson, and J. H. Reed, “Semidefinite relaxation-based PAPR-aware precoding for massive MIMO-OFDM systems,” *IEEE Trans. Veh. Technol.*, vol. 68, no. 3, pp. 2229–2243, Oct. 2019.
- [21] R. Zayani, H. Shaiek, and D. Roviras, “PAPR-aware massive MIMO-OFDM downlink,” *IEEE Access*, vol. 7, pp. 25 474–25 484, Feb. 2019.
- [22] S. Taner and C. Studer, “ $\ell^p - \ell^q$ -norm minimization for joint precoding and peak-to-average-power ratio reduction,” *arXiv:2107.06986*, Oct. 2021.
- [23] S. P. Boyd and L. Vandenberghe, *Convex optimization*. Cambridge University Press, 2004.
- [24] 3GPP TS 38.104, “NR; Base station (BS) radio transmission and reception,” V15.4.0, 2021.
- [25] P. L. Combettes and J.-C. Pesquet, “Proximal splitting methods in signal processing,” in *Fixed-Point algorithms for inverse problems in science and engineering*. Springer, New York, NY, 2011, pp. 185–212.
- [26] S. Boyd, N. Parikh, E. Chu, B. Peleato, and J. Eckstein, “Distributed optimization and statistical learning via the alternating direction method of multipliers,” *Foundations and Trends® in Machine Learning*, vol. 3, no. 1, pp. 1–122, 2011.
- [27] N. Parikh, S. Boyd, N. Parikh, and S. Boyd, “Proximal algorithms,” *Foundations and Trends® in Optimization*, vol. 1, no. 3, pp. 123–231, 2013.
- [28] H. Wang and A. Banerjee, “Bregman alternating direction method of multipliers,” in *Proc. Adv. Neural Inf. Process. Syst.*, 2014, pp. 2816–2824.
- [29] N. Komodakis and J. Pesquet, “Playing with duality: An overview of recent primal-dual approaches for solving large-scale optimization problems,” *IEEE Signal Process. Mag.*, vol. 32, no. 6, pp. 31–54, Oct. 2015.
- [30] R. Glowinski, S. J. Osher, and W. Yin, *Splitting methods in communication, imaging, science, and engineering*, ser. Scientific Computation. Cham, Switzerland: Springer International Publishing, 2016.
- [31] A. Beck, *First-order methods in optimization*. SIAM, 2017.
- [32] D. Davis and W. Yin, “A three-operator splitting scheme and its optimization applications,” *Set-Valued and Variational Analysis*, vol. 25, no. 4, pp. 829–858, Dec. 2017.
- [33] M. Yan, “A new primal-dual algorithm for minimizing the sum of three functions with a linear operator,” *J. Sci. Comput.*, vol. 76, pp. 1698–1717, 2018.
- [34] E. K. Ryu and W. Yin, *Large-scale convex optimization via monotone operators*. Cambridge University Press (to be published), 2022.
- [35] S. Kant, M. Bengtsson, B. Göransson, G. Fodor, and C. Fischione, “Efficient optimization for large-scale MIMO-OFDM spectral precoding,” *IEEE Trans. Wireless Commun.*, vol. 20, no. 9, pp. 5496–5513, Sep. 2021.
- [36] S. Banert, R. I. Boş, and E. R. Csetnek, “Fixing and extending some recent results on the ADMM algorithm,” *Numerical Algorithms*, pp. 1–23, May 2020.
- [37] P. L. Combettes and J.-C. Pesquet, “Fixed point strategies in data science,” *IEEE Trans. Signal Process.*, pp. 1–1, 2021.
- [38] S. Kant, M. Bengtsson, G. Fodor, B. Göransson, and C. Fischione, “EVM-constrained and mask-compliant MIMO-OFDM spectral precoding,” *IEEE Trans. Wireless Commun.*, vol. 20, no. 1, pp. 590–606, Jan. 2021.
- [39] N. N. Moghadam, G. Fodor, M. Bengtsson, and D. J. Love, “On the energy efficiency of MIMO hybrid beamforming for millimeter-wave systems with nonlinear power amplifiers,” *IEEE Trans. Wireless Commun.*, vol. 17, no. 11, pp. 7208–7221, Nov. 2018.
- [40] E. G. Larsson and L. Van Der Perre, “Out-of-band radiation from antenna arrays clarified,” *IEEE Wireless Commun. Lett.*, vol. 7, no. 4, pp. 610–613, Aug. 2018.
- [41] N. N. Moghadam, P. Zetterberg, P. Händel, and H. Hjalmarsson, “Correlation of distortion noise between the branches of MIMO transmit antennas,” in *Proc. IEEE Int. Symp. Pers., Indoor, Mobile Radio Commun. (PIMRC)*, Sep. 2012, pp. 2079–2084.

- [42] E. Sienkiewicz, N. McGowan, B. Göransson, T. Chapman, and T. Elfström, "Spatially dependent ACLR modelling," in *Proc. IEEE Conf. Antenna Meas. Appl. (CAMA)*, Nov. 2014, pp. 1–4.
- [43] R. Hassun, M. Flaherty, R. Matreci, and M. Taylor, "Effective evaluation of link quality using error vector magnitude techniques," in *Proc. IEEE Wireless Commun. Conf.*, 1997, pp. 89–94.
- [44] H. A. Mahmoud and H. Arslan, "Error vector magnitude to SNR conversion for nondata-aided receivers," *IEEE Trans. Wireless Commun.*, vol. 8, no. 5, pp. 2694–2704, May 2009.
- [45] H. H. Bauschke and P. L. Combettes, *Convex analysis and monotone operator theory in Hilbert spaces*, ser. CMS Books in Mathematics. New York, NY: Springer New York, 2011.
- [46] S. Kant, M. Bengtsson, G. Fodor, B. Göransson, and C. Fischione, "An introduction to three-operator ADMM for wireless communications and machine learning," *under preparation*, 2022.
- [47] M. Grant and S. Boyd, "CVX: Matlab software for disciplined convex programming, version 2.1," <http://cvxr.com/cvx>, Mar. 2014.
- [48] Y. Sun, P. Babu, and D. P. Palomar, "Majorization-Minimization algorithms in signal processing, communications, and machine learning," *IEEE Trans. Signal Process.*, vol. 65, no. 3, pp. 794–816, 2017.
- [49] 3GPP TR 38.901, "Study on channel model for frequencies from 0.5 to 100 GHz," V16.1.0, 2020.
- [50] 3GPP TS 38.101-4, "User equipment (UE) radio transmission and reception; part 4: Performance requirements," V15.10.0, 2021.
- [51] E. Bala, J. Li, and R. Yang, "Shaping spectral leakage: A novel low-complexity transceiver architecture for cognitive radio," *IEEE Veh. Technol. Mag.*, vol. 8, no. 3, pp. 38–46, Jul. 2013.
- [52] N. Fatema, G. Hua, Y. Xiang, D. Peng, and I. Natgunanathan, "Massive MIMO linear precoding: A survey," *IEEE Systems Journal*, vol. 12, no. 4, pp. 3920–3931, Dec. 2018.